REVIEW

CHEMISTRY

Special Topic: Energy Storage Materials

Pseudocapacitive materials for electrochemical capacitors: from rational synthesis to capacitance optimization

Jie Wang[1,†], Shengyang Dong[1,†], Bing Ding[1], Ya Wang[1], Xiaodong Hao[1], Hui Dou[1], Yongyao Xia[2] and Xiaogang Zhang[1,*]

ABSTRACT

Among various energy-storage devices, electrochemical capacitors (ECs) are prominent power provision but show relatively low energy density. One way to increase the energy density of ECs is to move from carbon-based electric double-layer capacitors to pseudocapacitors, which manifest much higher capacitance. However, compared with carbon materials, the pseudocapacitive electrodes suffer from high resistance for electron and/or ion transfer, significantly restricting their capacity, rate capability and cyclability. Rational design of electrode materials offers opportunities to optimize their electrochemical performance, leading to devices with high energy density while maintaining high power density. This paper reviews the different approaches of electrodes striving to advance the energy and power density of ECs.

Keywords: electrochemical capacitors, pseudocapacitive electrode, energy density, power density, cycle stability

[1]Key Laboratory of Materials and Technologies for Energy Conversion, College of Material Science & Engineering, Nanjing University of Aeronautics and Astronautics, Nanjing, 210016, China and [2]Department of Chemistry and Shanghai Key Laboratory of Molecular Catalysis and Innovative Materials, Institute of New Energy and iChEM (Collaborative Innovation Center of Chemistry for Energy Materials), Fudan University, Shanghai, 200433, China

[†]Equally contributed to this work.

[*]**Corresponding author.** E-mail: azhangxg@nuaa.edu.cn

INTRODUCTION

The fast development of industry has triggered serious global warming and the lack of fossil fuels, which pose significant threats to the survival and development of mankind. To address these issues, scientists and engineers have been conducting intense research efforts into the design and fabrication of efficient energy-conversion and storage devices to exploit sustainable and clean energy. In this regard, electrochemical capacitors (ECs), lithium-ion batteries (LIBs) and fuel cells are recognized as three kinds of the most important electrochemical energy-storage/conversion devices.

Among them, ECs, also known as supercapacitors or ultracapacitors, have drawn considerable attention during recent years due to their distinct power density (fast charging/discharging within seconds) and prominent life cycle ($>10^6$ cycles) when compared to batteries and fuel cells (Fig. 1) [1–3]. However, the relatively low energy density of ECs greatly restricts their application in energy-requiring equipment. The maximum energy (E) accumulated in EC is directly proportional to the capacitance (C) and the square of applied voltage (V^2) according to the equation:

$$E = \frac{1}{2}CV^2 \qquad (1)$$

while the power density (P) is given by the equation:

$$P = \frac{V^2}{4ESR \bullet m}, \qquad (2)$$

where *ESR* represents the equivalent series resistance and m represents the total mass of the two electrodes. Therefore, on the one hand, the energy-density enhancement can be achieved by developing electrode material with high capacitance. Pseudocapacitive electrode materials, mainly metal oxides, metal sulfides and conducting polymers, are considered as promising electrode materials, as their capacitance usually far exceeds the double-layer capacitance achievable with carbon materials [4].
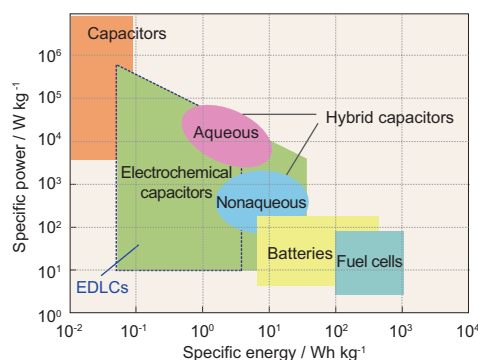
Figure 1. Ragone plot with specific energy and power for different energy-storage devices.

Another approach is to widen the operational window by using non-aqueous electrolyte or by constructing hybrid capacitors, which combine a faradic electrode and a porous carbon electrode in a device [5]. Therefore, both of these methods require high-performance faradic electrodes. Pseudocapacitive electrode materials, however, usually suffer from low conductivity, leading to a large *ESR*. The power capability is thus dramatically determined. In addition, the low electrolyte-accessible surface area restricts the pseudocapacitive process occurring at the electrode/electrolyte interface. Furthermore, the irreversible change that occurs during the chemical reaction will shorten the life cycle of the electrode materials. Accordingly, the development of pseudocapacitors and hybrid capacitors is driven by the desire to increase the specific energy while retaining the high power and long-term cyclability.

In this review, we mainly discuss the recent research activities carried out with an emphasis on the rational design of pseudocapacitive electrodes for ECs as well as their electrochemical performance. This review is organized into three sections: (i) overview of ECs and pseudocapacitive electrode materials; (ii) the recent development in preparing electrode materials based on redox reactions; (iii) the recent development in preparing electrode materials based on intercalation reactions. We aim to outline the benefits and challenges of the use of pseudocapacitive electrode materials in ECs. We also highlight the key technical challenges with the hope of stimulating further advances in research.

FUNDERMENTALS OF ECS
Principle of electrochemical capacitors

Conventional capacitors, namely dielectric capacitors, are governed by the principle of charge separation in an electric field in the dielectric oxide layer between two electrodes [1]. Typically, the capacitance

(C_{dl}) of conventional capacitors can be calculated by the equation:

$$C_{dl} = \frac{\varepsilon_0 \varepsilon_r A}{D}, \qquad (3)$$

where ε_0 is the permittivity of free space, ε_r is the dielectric constant (or relative permittivity) of the material between the plates, A is the area of each electrode and D is the distance between the electrodes. Because of their limited area (A) and large distance (D), conventional capacitors can only provide minuscule capacity to store charge and have never been considered as energy-storage devices. Then the concept of electric double-layer capacitors (EDLCs), which utilize the electric charge accumulated at the carbon electrode surface and ions of the opposite to store energy, provide energy density higher by orders of magnitude than conventional capacitors for a given device size. The greatly improved energy density results from the enhanced active area of electrodes and the minimal magnitude of charge separation (D) down to a few Angstroms. Yet, due to the pure physical process that occurs on the surface of the electrode, an EDLC exhibits high rate capability but limited capacitance compared with a battery.

Until 1971, pseudocapacitors (PCs), which store charge through the transfer of charge between electrode and electrolyte, was discovered [6]. The pseudocapacitance (C_{pc}) is proportional to the charge transferred in this process, which can be described by the equation:

$$C_{pc} = q\left(\frac{d\theta}{dV}\right), \qquad (4)$$

where q is the faradic charge required for adsorption/desorption of ions, $d\theta$ is the change in fractional coverage of the surface and dV is the change in potential [7]. Since the value of $d\theta/dV$ is not entirely linear, the capacitance is not always constant and so it is called pseudocapacitance. The faradic process enables PCs to achieve much higher energy density and specific capacitance than EDLCs. According to Conway's research, the faradic process of PCs can result from the following three mechanisms [1]: (i) underpotential deposition, (ii) redox pseudocapacitance and (iii) intercalation pseudocapacitance (Fig. 2). Underpotential deposition occurs when metal ions form an absorbed monolayer on a different metal's surface well above their redox potential. The redox reaction is a 'surface charge storage' process realized by electrochemical adsorption of ions on/near the surface and a successive electron transfer at redox active sites. Metal oxides, metal sulfides, metal nitrides, metal hydroxides and conducting polymers are well-known examples of pseudocapacitive materials. The intercalation
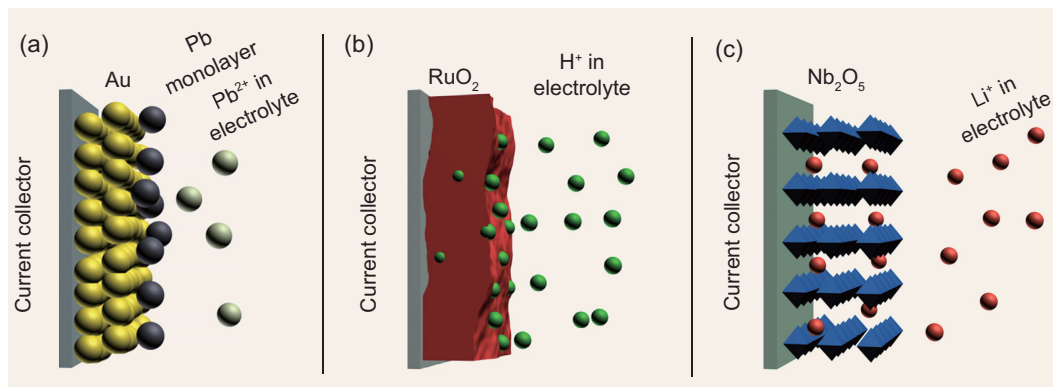
Figure 2. Different types of reversible redox mechanisms that give rise to pseudocapacitance: (a) underpotential deposition, (b) redox pseudocapacitance and (c) intercalation pseudocapacitance.

pseudocapacitance is based on the intercalation of electroactive species in the layer without crystallographic phase change. In this case, the most investigated insertion-type electrodes involve V_2O_5, Nb_2O_5 and so on. Redox and intercalation pseudocapacitances are more frequently exploited in the design of PCs. Notably, both of these two faradic processes display very fast charge/discharge rates without diffusion limitation. This is the most obvious distinction from batteries, which are limited by solid-state diffusion and suffer from a poor rate capability.

To better understand the kinetic behavior of electrodes, it is important to separate the capacitive and diffusion contributions of pseudocapacitive material in an electrochemical process. In the next section, we will discuss the electrochemical features of pseudo-capacitance.

Important parameters of EC electrodes

Recently, analysis of cyclic voltammetry (CV) curves has been the prevailing method for distinguishing the particular features of pseudocapacitive materials. In a CV test, the current response to an applied sweep rate is different, depending on whether the redox reaction is surface-controlled (capacitive) or diffusion-controlled (battery) [8]. The relationship can be expressed by the equation:

$$i(V) = k_1 \upsilon^{1/2} + k_2 \upsilon, \tag{5}$$

where υ is scan rate (mV/s). For a capacitive process on the surface, the current response varies directly with υ. For a process limited by the semi-infinite linear diffusion, the current varies with $\upsilon^{1/2}$. Calculating the values of k_1 and k_2 at each potential will give the contribution of the capacitive or diffusion process. The relationship between capacity and scan rate can also be used to analyse the electrochemical process [9], which can be described by the equation:

$$Q = Q_{\upsilon=\infty} + \text{constant}(\upsilon^{-1/2}). \tag{6}$$

In this equation, the capacitive contribution is represented by $Q_{\upsilon=\infty}$ while the diffusion-controlled capacity is limited by $\upsilon^{1/2}$. By plotting the curve of capacity *vs.* $\upsilon^{1/2}$, the contribution of the outer surface and the bulk solid can be distributed. Another feature expressed in the CV curve is the relationship between the peak potential and the scan rate. In a capacitive system, there should be a small or no potential difference between the anodic and cathodic peaks in the CV curves, especially at low scan rates, which means that this process is reversible [10].

Galvanostatic charge/discharge curves and impedance spectroscopy can also be used to characterize the pseudocapacitive behavior. In the galvanostatic charge/discharge curves, the pseudocapacitive process without phase change is indicated by a linear-shaped profile of potential *vs.* capacity. In addition, the voltage hysteresis between the charging and discharging steps is very small. These characteristics are totally different from those of batteries, which manifest an obvious voltage plateau in charge/discharge curves. An ideal capacitor should show an activated carbon (AC) impedance result as a vertical line with a 90° angle, while pseudocapacitive behavior will show a phase angle of <90°. This relationship can be represented by a constant-phase element in the equivalent circuit equation:

$$Z = \frac{1}{B(i\omega)^p}. \tag{7}$$

When p is 1, this indicates an ideal capacitor and, when p is 0.5, this indicates semi-infinite diffusion.

In some cases, some materials do not show characteristic pseudocapacitive behavior in bulk, but do in nanostructured states. This kind of material is
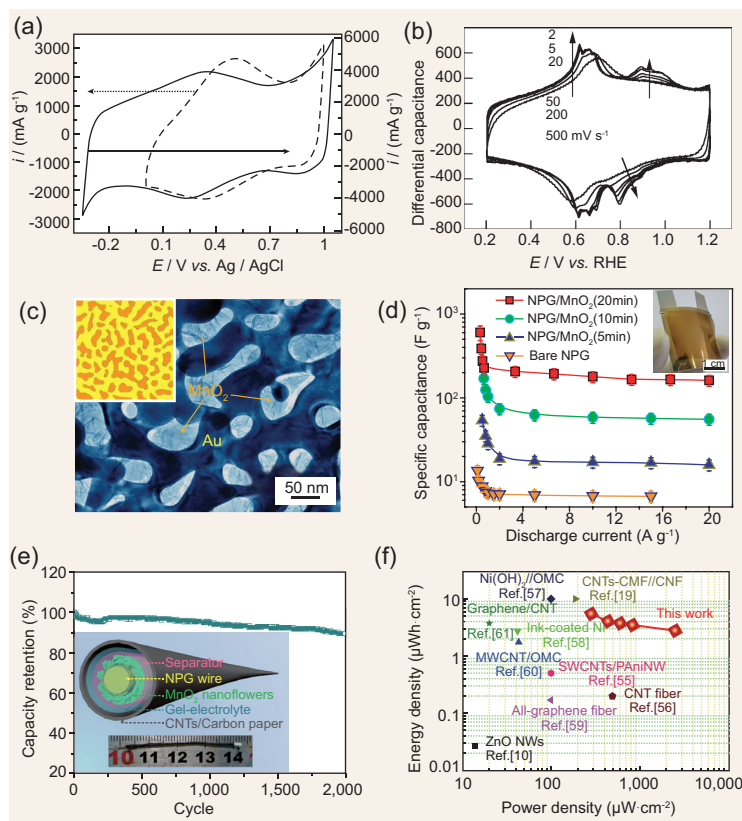
Figure 3. (a) Voltammetric behavior of AC-RuO$_x$/G electrodes; where RuO$_x \cdot$nH$_2$O (1) without (dotted line) and (2) with (solid line) annealing in air at 200°C for 2 h [13] (Copyright 2003, The Electrochemical Society). (b) Cyclic voltammograms of layered H$_{0.2}$RuO$_{2.1} \cdot$nH$_2$O. [14] (Copyright 2005, American Chemical Society). (c) Bright-field transmission electron microscopy (TEM) image of the nanoporous gold (NPG)/MnO$_2$ hybrid with a MnO$_2$ plating time of 20 min. Inset: Schematic illustration of directly growing MnO$_2$ (orange) onto NPG (Copyright 2011, Nature Publishing Group). (d) Specific capacitance *vs.* discharge current density for bare NPG electrodes and for NPG/MnO$_2$ electrodes with different plating times. Inset: Photograph of a NPG/MnO$_2$-based supercapacitor. (e) Cycling performance of the device measured at a current density of 0.6 mA/cm^2. Inset: Schematic diagram of a coaxial fiber ASC [15] (Copyright 2014, Springer). (f) Ragone plots of the device.

called an extrinsic electrode material. Otherwise, materials display the characteristics of capacitive charge storage for a wide range of particle sizes and morphologies and are called intrinsic materials. In the following sections, the electrochemical performance of various pseudocapacitive materials will be discussed according to the different pseudocapacitive mechanisms and on the basis of the key features presented above.

REDOX PSEUDOCAPACITIVE ELECTRODE MATERIALS

The most highly investigated materials as redox pseudocapacitive electrodes include transition metal oxides, metal hydroxides, metal sulfides, metal

nitrides and conducting polymers. Compared with carbon materials, this kind of material suffers from lower conductivity and low electrolyte-accessible surface area. Various strategies have been proposed for improving their performance, mainly including nanostructuration, deposition onto high-surface-area materials such as graphene, carbon nanotubes or porous carbons and combinations with highly conductive substrates.

Transition metal oxides

RuO$_2$, as the first investigated pseudocapacitive electrode material, has been extensively studied in acidic solution over the past 30 years [11–13]. During the charge/discharge process, rapid reversible electron transfer is accompanied by electroadsorption of protons on the surface RuO$_2$ particles, where Ru oxidation states can change from Ru($+2$) to Ru($+4$):

$$RuO_2 + xH^+ + xe^- \leftrightarrow RuO_{2-x}(OH)_x.$$
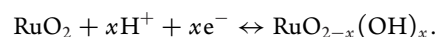
Owing to their high conductivity and the presence of structural water, the electrode materials can be highly utilized and the highest capacitance reported for hydrated RuO$_2$ reached 1340 F/g, which is close to its maximum theoretical value of 1400 F/g (Fig. 3a) [13]. Some researchers claim that only suitable aqueous electrolyte is RuO$_2$, since its high capacitance comes from the surface reaction between active ions and protons in strong acid electrolytes. Due to the good electrochemical reversibility, RuO$_2$ also demonstrates prominent rate capability. Upon increasing scan rates from 2 to 500 mV/s, the capacitance of RuO$_2$ can retain ~75% (Fig. 3b) [14], which is even comparable to most carbon materials. Presently, RuO$_2$ is still the most promising pseudocapacitive electrode for its remarkable electrochemical performance. Although the toxicity and high cost restrict the large-scale energy storage of RuO$_2$, it can still be used in some micro-devices for special purposes.

Some transition metal oxides which also exhibit pseudocapacitive behavior are anticipated to be low-cost alternatives to RuO$_2$ for ECs. However, due to their poor electronic conductivity, the charge storage is confined to a thin layer of the surface, resulting in a much lower capacitance than the theoretical value. In addition, the rate capability is also offset by the low charge-transfer kinetics intrinsic and sluggish ion diffusion to redox reaction. To improve the electrochemical property, one of the most effective strategies is to increase the surface area of the metal oxide to accommodate large amounts of superficial electroactive species to participate in

faradic redox reactions. For example, the capacitance in thick MnO_2 electrodes (ranging between 200 and 250 F/g) is much lower than the theoretical value due to the low active sites for charge transfer [16]. When MnO_2 electrodes are processed into ultrathin films, the ion-accessible surface area is greatly enhanced and the specific capacitance is dramatically increased to more than 1000 F/g [17]. Furthermore, constructing hybrid nanostructures of conductive matrix (metal or carbon) and metal oxides will be capable of further facilitating electron and proton conduction. Chen proposed a hybrid structure of nanoporous gold (NPG) and nanocrystalline MnO_2, in which the NPG allows electron transport through the MnO_2, and facilitates fast ion diffusion between the MnO_2 and the electrolyte (Fig. 3c). A high capacitance of ~1,145 F/g was achieved, which is very close to the theoretical value (Fig. 3d) [18]. Recently, Hu *et al.* used NPG wires as flexible supports to grow MnO_2 nanoflowers, which not only enables full utilization of MnO_2 and fast electronic/ionic transfer through the electrode, but also avoids using a binder. By scrolling a carbon nanotube (CNT)/carbon paper electrode on the NPG@MnO_2 wire electrode with a polymer gel, a novel design of an all-solid-state, highly flexible, coaxial fiber asymmetric supercapacitor (ASC) was made (Fig. 3e). The as-fabricated coaxial fiber ASCs can be reversibly charged/discharged at a high voltage of 1.8 V, delivering a satisfactory energy density of 5.4 μWh/cm^2 and a maximum power density of 2531 μW/cm^2 (Fig. 3f) [15]. Owing to the partial dissolution of MnO_2 in the electrolyte, however, MnO_2 suffers from capacitance degradation during cycling, which restricts its wide application.

In recent years, spinel metal oxides (NiO, Co_3O_4, Fe_3O_4, Mn_3O_4 and mixed transition metal spinels such as $NiCo_2O_4$ and $MnFe_2O_4$) have been considered as promising high-performance pseudocapacitive active materials for their high theoretical capacitance (>3000 F/g) [19,20,23–29]. Take Co_3O_4, for example; the pseudocapacitance originates from the following redox reactions:

$$Co_3O_4 + H_2O + OH^- \leftrightarrow 3CoOOH + e^-.$$
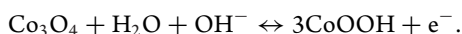
Nanosized and nanostructured electrode materials have been widely employed to increase the surface area to enhance the pseudocapacitance. In addition, the hierarchically porous structure (macro/mesopore) of the electrode materials is also critical to ease the mass transfer of electrolytes for fast redox reactions. Zhang and Yuan *et al.* successfully prepared hierarchical porous NiO and Co_3O_4 with nano/micro spherical superstructures which demonstrate high capacitances [23,30]. But, re-

stricted by the intrinsic low conductivity, the capacitances are far beyond the theoretical value. To improve the electron transfer, Zhang *et al.* directly grew the nanostructured Co_3O_4 on nickel foam through a hydrothermal method, which can be directly applied as self-supported electrodes for ECs. The resulting active materials exhibited a high specific capacitance of 1160 F/g at 2 A/g and remarkable rate capability, even remaining at 820 F/g at 20 A/g (Fig. 4a) [19]. Shen reported an advanced electrode architecture consisting of carbon textiles uniformly covered by mesoporous $NiCo_2O_4$ nanowire arrays. With a high surface area, a high specific capacitance of 1010 F/g (79% of the capacitance at 1 A/g) at 20 A/g and prominent cycling stability (no specific capacitance decay after 5000 cycles at 8 A/g) were achieved [26]. However, the problem with these methods is the relatively low weight fraction of the pseudocapacitive material, which will sacrifice the energy density of the full device. Some efforts then were directed at growing hybrid pseudocapacitive materials, both of which are high-capacitance electrode materials, on conductive substrate [20,21,31]. Fan constructed Co_3O_4@MnO_2 core–shell arrays with a Co_3O_4 nanowire core and ultrathin MnO_2 shell directly on the current collector (Fig. 4b) [20]. The porous structure and the ordered array geometry enhanced the surface area for the redox reaction and shortened the ion diffusion path. The obtained Co_3O_4@MnO_2 hybrid nanowire array exhibited ~4–10-fold increased areal capacitance with respect to the pristine Co_3O_4 array, with good cycle performance (2.7% capacitance loss after 5000 cycles) and remarkable rate capability (56% capacitance retention at a very large current density of 44.7 mA/cm^2, charge/discharge within 7 s) (Fig. 4c). Liu deposited cobalt and nickel double hydroxide nanosheets on porous $NiCo_2O_4$ nanowires which were radially grown on carbon fiber [21]. This hybrid composite electrode also exhibited excellent rate capability; the areal capacitance decreased by less than 33% as the current density increased from 2 to 90 mA/cm^2, offering excellent specific energy density (~33 Wh/kg) and power density (~41.25 kW/kg) at high cycling rates (up to 150 mA/cm^2) (Fig. 4d).

Recently, several studies used *in situ* and *ex situ* characterization to analyse the charge-storage process that occurred on the surface of metal oxides [25,28]. It was indicated that the ion disproportionation and morphology collapse are the main reasons for the capacity change during cycling. Therefore, strategies which could solve these problems are needed. In addition, according to Equations (5–7), some spinel materials exhibit both capacitive and battery-type behavior due to phase changes involved
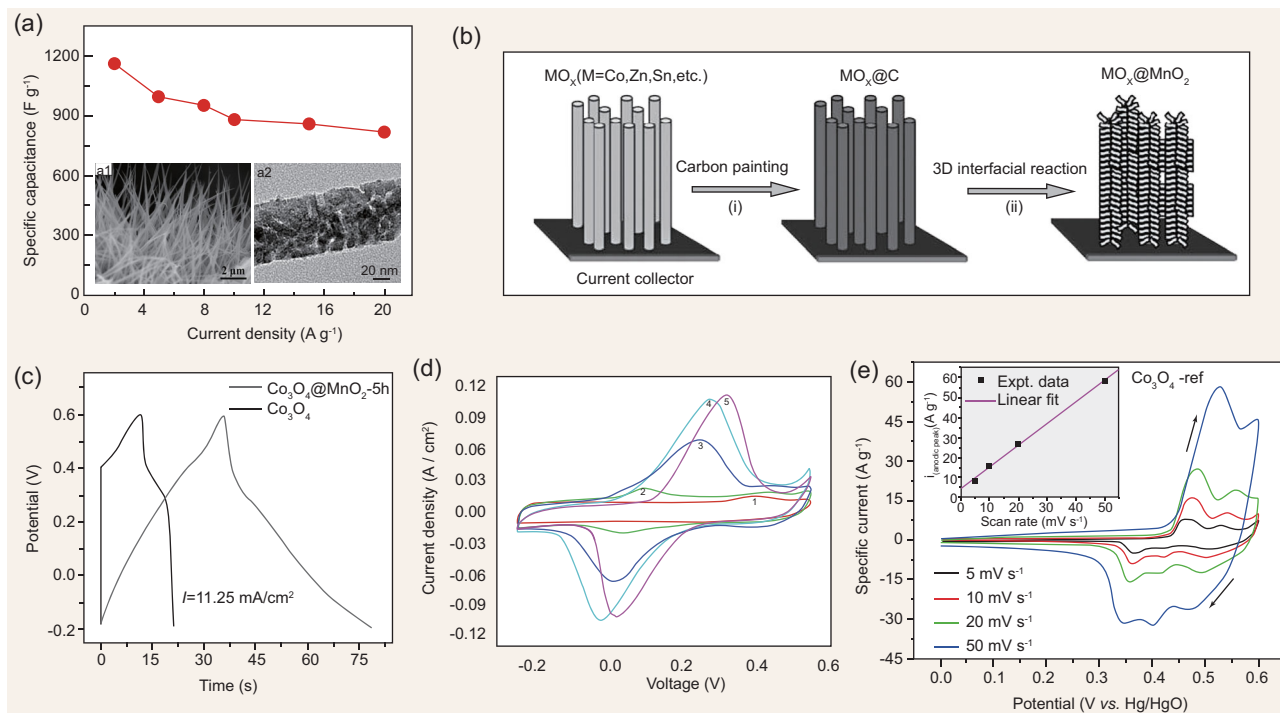
Figure 4. (a) Rate performance of Co_3O_4 NW array. Insets: The (a1) scanning electron microscopy (SEM) image and (a2) TEM image of Co_3O_4 NW [19] (Copyright 2012, Elsevier Limited). (b) Schematic illustration of the general electrode design process of $MO_x@MnO_2$ arrays [20] (Copyright 2011, John Wiley & Sons, Inc.). (c) Charge/discharge curves for 5-h-grown hybrid nanowire array and pristine Co_3O_4 array. (d) CVs of $NiCo_2O_4$/CFP and hybrid composite at a scan rate of 20 mV/s: (1) $NiCo_2O_4$/CFP; (2) Co DHs/$NiCo_2O_4$/CFP; (3) $Co_{0.67}Ni_{0.33}$ DHs/$NiCo_2O_4$/CFP; (4) $Co_{0.5}Ni_{0.5}$ DHs/$NiCo_2O_4$/CFP; (5) $Co_{0.33}Ni_{0.67}$ DHs/$NiCo_2O_4$/CFP [21] (Copyright 2013, American Chemical Society). (e) CV of the Co_3O_4-ref at different scan rates [22] (Copyright 2011, American Chemical Society).

during charge/discharge (Fig. 4e) [22]. Therefore, the capacitance was increased but the rate capability was sacrificed. In order to understand the charge-storage process in these materials, it is important to use various analyses of kinetics to separate the capacitive and diffusion contributions in spinel metal oxides in future research.

Transition metal sulfides

Transition metal sulfides, such as cobalt sulfides (CoS_x) and nickel sulfides (NiS_x), are receiving more and more attention as electrode materials for supercapacitors due to their remarkable electrochemical capacitive performance in alkaline electrolyte solutions [32,33]. Tao *et al.* first synthesized the amorphous cobalt sulfide (CoS_x) by a simple chemical precipitation method and employed it for ECs [32]. This material showed a high specific capacitance of 369 F/g at a current density of 50 mA/cm^2. The possible reaction can be expressed in the following equations:

$$CoS + OH^- \leftrightarrow CoSOH + e^-$$

$$CoSOH + OH^- \leftrightarrow CoSO + H_2O + e^-.$$
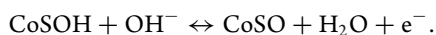
Lou *et al.* further used the hydrothermal method to synthesize hierarchical NiS hollow spheres, which manifested interesting supercapacitive properties of 927 F/g at 4.08 A/g and 618 F/g at 8.16 A/g [33]. Despite the high capacitance, the metal sulfides suffer from inferior cycling performance. It may be the result of some irreversible redox reaction which can be observed from the large potential difference between the anodic and cathodic peaks in the CV curves. Combing with carbon materials or synthesizing materials directly on current collectors may be an effective strategy to solve this problem. For example, bacteria-reduced graphene oxide (rGO)-nickel sulfide networks were prepared by deposition rGO/Ni_3S_2 nanoparticle composites directly onto substrate [34], which promoted the capacitance to 1424 F/g at 0.75 A/g and 961 F/g at 15 A/g. After 3000 charge/discharge cycles, 89.6% of the initial capacitance remained.

Ternary nickel cobalt sulfides have been regarded as a promising class of electrode materials for high-performance energy-storage devices, since they offer higher electronic conductivity ($\sim$100 times as high as that of $NiCo_2O_4$), electrochemical activity and larger capacity than mono-metal sulfides [35–37]. Shen and Yu reported on $NiCo_2S_4$ ball-in-ball
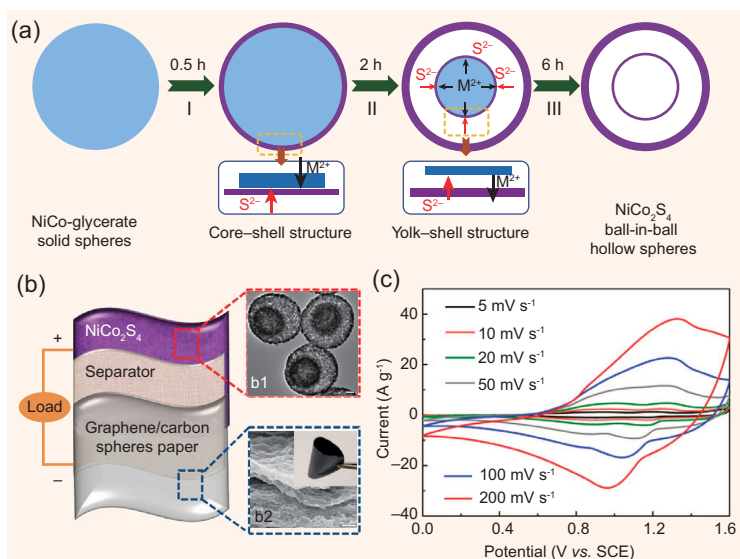
Figure 5. (a) Schematic illustration of the formation process of NiCo$_2$S$_4$ ball-in-ball hollow spheres [18] (Copyright 2016, Nature Publishing Group). (b) Schematic illustration of the asymmetric supercapacitor device. The insets show the (b1) TEM image of NiCo$_2$S$_4$ ball-in-ball hollow spheres and (b2) SEM image of G/CS paper. Scale bar, b1: 100 nm; b2: 1 μm. (c) CV curves of the asymmetric supercapacitor device at different scan rates.

hollow spheres which deliver a specific capacitance of 1036 F/g at a current density of 1.0 A/g (Fig. 5a). An asymmetric supercapacitor based on these ball-in-ball structures shows long-term cycling performance with a high energy density of 42.3 Wh/kg at a power density of 476 W/kg [35] (Fig. 5b and c). The excellent electrochemical performance should be attributed to the complex NiCo$_2$S$_4$ hollow structure, enabling high porosity, enlarged active surface area and improved structural integrity. Alshareef *et al.* prepared Ni—Co—S interconnected nanosheet arrays on conductive carbon substrates as free-standing electrodes for supercapacitors. Taking advantage of the highly conductive, mesoporous structure in the nanosheets and open framework of the 3D nanoarchitectures, the Ni—Co—S electrodes exhibit high specific capacitance (1418 F/g at 5 A/g) with outstanding rate capability (1285 F/g at 100 A/g) as well as robust long-term cycling stability [36]. The excellent pseudocapacitive performance of ternary sulfides indicates that they may be a kind of prominent electrode material. But, until now, the exact reaction mechanism of metal sulfide has not been verified, and a deep study of electrochemical capacitive behavior needs to be made.

Metal nitrides nanomaterials

Transition metal nitrides are traditionally known for their characteristics of high melting points and chemical stability against acids and bases. The at-

tention to metal nitrides as pseudocapacitive electrodes was first paid by Finello and Roberson with an investigation on molybdenum nitrides (MoN), which demonstrated wide operation windows, large capacitance and remarkable stability in acidic electrolytes [8]. In recent years, this work has been revisited using other metal nitrides, such as vanadium nitride (VN), titanium nitride (TiN) and so on, due to their attractive electrical conductivity, which enables them to compete with metal oxide-based electrode materials. According to the report by Choi *et al.*, VN has shown an exceptional capacitance of up to 1340 F/g, albeit with a very low mass loading [38]. The energy-storage mechanism of VN has been attributed to a combination of both double-layer-type capacitance and the pseudocapacitance response of the thin amorphous surface oxide grown on the surface of VN (Fig. 6a) [38,39]. Nevertheless, the following studies on VN as a capacitive electrode only manifested capacitances of 50~200 F/g [40–42]. Kumta and co-workers thoroughly investigated the different electrochemical behaviors of nanostructured VN prepared through mechanical milling and VN nanocrystalline was reported by Choi [42]. It is indicated that, in spite of the different mass loading, the oxidation state of V on the surface, specific surface area (SSA) and size of nanoparticles are serious issues for the capacitance of VN. To further improve the capacitance and rate performance of VN, nanostructures involving CNT/VN composite or core–shell VN/TiN were prepared [41,43]. Zhang *et al.* prepared ternary vanadium titanium nitride/carbon nanofibers (VTiN/C) as promising novel supercapacitor electrodes (Fig. 6b) [44]. By using the synergistic effect of V and Ti, the fabricated VTiN/C exhibited an impressive capacitance of 430.7 F/g at 1 A/g and excellent rate capability (141.7 F/g at 10 A/g), which far exceeded pure VN or TiN nanofibers (Fig. 6c). These encouraging results suggested that ternary metal nitrides are promising electrode materials for supercapacitors. Metal nitrides are instable, however, in aqueous electrolyte due to the irreversible electrochemical oxidation process of forming VO$_x$ on the surface. Tong and Li *et al.* proposed to construct a quasi-solid-state asymmetric supercapacitor using VN nanowire as the anode, VO$_x$ as the cathode and LiCl/PVA as the gel electrolyte (Fig. 6d) [45]. The VO$_x$//VN asymmetric supercapacitor exhibited a stable operational window of 1.8 V and prominent cycling stability with only 12.5% degradation of capacitance after 10 000 cycles. In addition, the VO$_x$//VN device exhibited impressive mechanical flexibility, demonstrated by a stable electrochemical performance without any change under different bent conditions (Fig. 6e and f).
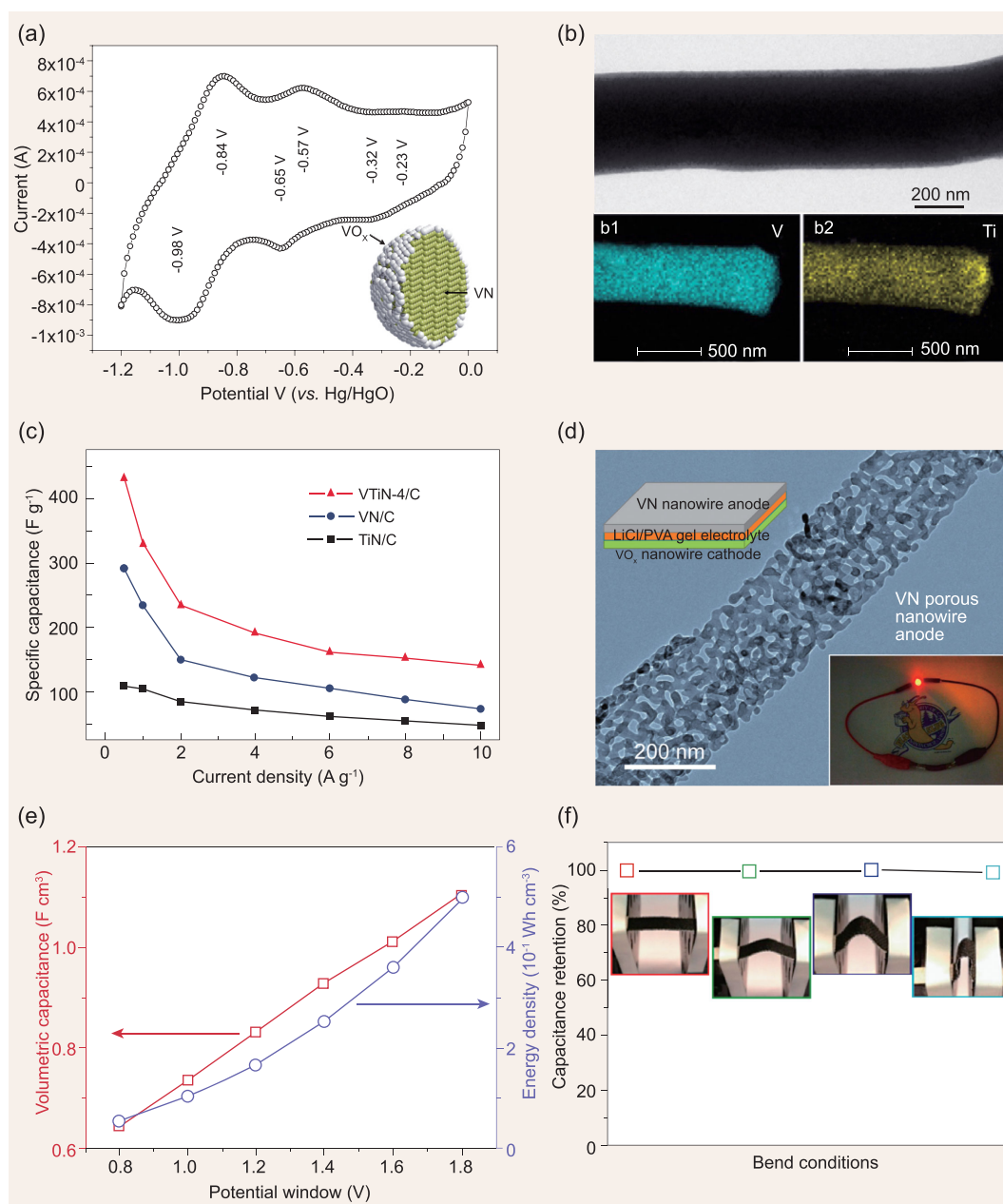
Figure 6. (a) CV of VN nanocrystals synthesized at 600°C scanned at 2 mV/s in 1 M KOH electrolyte. Inset: Illustration for modification of the surface chemistry of nanocrystalline VN [38] (Copyright 2006, John Wiley & Sons, Inc.). (b) TEM image of a single nanofiber with (b1–b2) elemental mapping of VTiN-4/C nanofibers [44] (Copyright 2015, John Wiley & Sons, Inc.). (c) Specific capacitance dependence on the current density collected from VN/C, TiN/C and VTiN-4/C samples. (d) TEM image of a porous VN nanowire [45] (Copyright 2013, American Chemical Society). (e) Volumetric capacitance and energy density calculated for the VO_x//VN-ASC device based on galvanostatic charge—discharge curves collected at 4 mA/cm² as a function of potential window. (f) Capacitance retention of the VO_x//VN-ASC device measured at different bent conditions. Insets: Pictures of the device.

Albeit with the development of metal nitrides, there is still no determination of their intrinsic behavior. Studies combining electrochemical techniques and various spectrometric methods may be needed to elucidate it. In addition, more efficient and controllable nitridation methods other than high-temperature gas-phase nitridation reactions need to be developed. Furthermore, some nitrides are worthy of study as potential pseudocapacitive electrodes. For example, a boron nitride/rGO composite with a superlattice structure was reported to achieve a high specific capacitance of 824 F/g at 4 A/g, which is very inspiring [46].
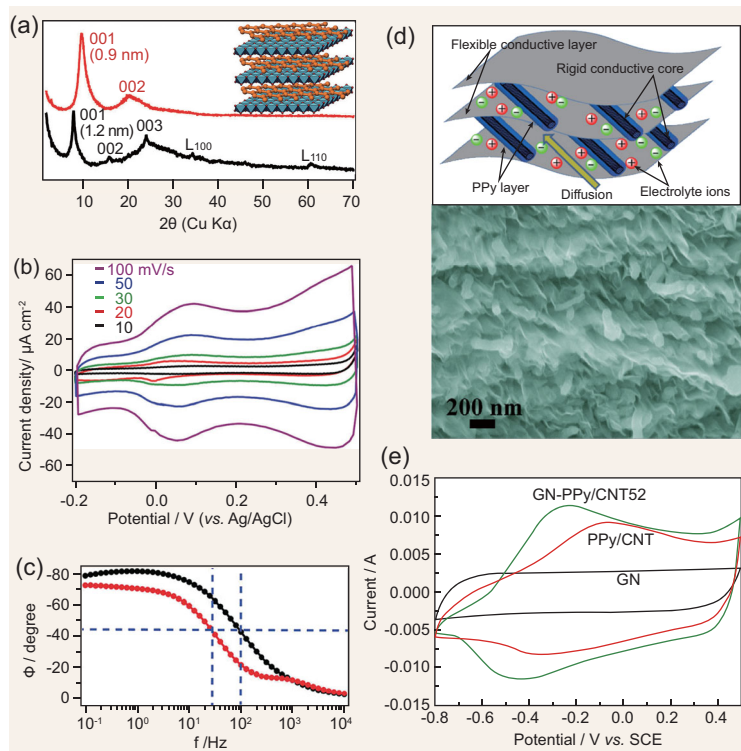
Figure 7. (a) X-ray diffraction (XRD) patterns of LDH nanosheets flocculated with GO (black trace) and rGO (red trace) nanosheets, respectively. Indices 00l are basal series of superlattice lamellar composites whereas L_{100} and L_{110} are in-plane diffraction peaks from LDH nanosheets. Inset: Schematic illustration of sandwiched LDH nanosheets and graphene [55] (Copyright 2014, John Wiley & Sons, Inc.). (b) CV curves of Co–Al LDH and rGO nanosheet composites at different scan rates. (c) Bode plots at different potentials of 0.1 V (red traces) and −0.1 V (black traces). (d) Schematic representation of the microstructure and energy-storage characteristics of the GN-PPy/CNT52 film and SEM image of cross-section of GNPPy/CNT52 [56] (Copyright 2012, Elsevier Limited). (e) CV curves of GN, PPy/CNT and GN-PPy/CNT52 within potential range of −0.8 to 0.5 V at scan rates of 10 mV/s in 1 M KCl.

Layered double hydroxides

Layered doublehydroxides (LDHs) are a kind of typical 2D nanostructured lamellar compound, which can be described by a generic formula $[M^{2+}_{1-x}M^{3+}_x(OH)_2][A^{n-}]_{x/n} \bullet zH_2O$, where M^{2+} and M^{3+} represent bivalent and trivalent metal cations, respectively; A^{n-} represents a charge-balancing anion; and x is generally in the range 0.2−0.4 [47−49]. Typically, LDHs are made of heterogeneous metal cations at unsaturated state in the host layer and ion-accessible interlayer spacing. When used as PC electrodes, the high electroactivity enables them with large theoretical capacitance, and the stable structure ensures prominent cyclability. The first report related to LDHs as electrode materials was a highly oriented and densely packed thin-film electrode by drying a transparent colloidal suspension of CoAl-LDH nanosheets on an Indium-Tin Oxide (ITO) substrate [47]. The thin-film electrode exhibits superior pseudocapacitive

behavior in terms of a large specific capacitance of 2000 F/cm^3 (667 F/g), good cycling stability and a high rate capability. Then, various methods, including *in situ* growth, electrodeposition, coprecipitation and so on, have been adopted to prepare LDH materials [50]. Literature survey indicates that a high surface area with a hierarchically porous structure is serious in improving the electrochemical performance of LDHs [51–53]. For example, Wei *et al.* fabricated core–shell NiAl-LDH microspheres with a high SSA (124.7 m^2/g) and tunable interior architecture using an *in situ* growth method. The hollow LDH microspheres exhibited a high specific capacitance of 735 F/g at 2 A/g and good rate capability (75% capacitance retention at 25 A/g), as well as a long-term cycling life (the capacitance increase by 16.5% after 1000 cycles at 8 A/g) [53]. In addition, adjustment of the metal proportion in LDHs will have an influence on the active sites for redox reaction, thus affecting the capacity and rate capability. For example, partial isomorphous substitution of Co^{2+} by Al^{3+} in Co$_{0.5}$Al$_{0.5}$-LDH leads to a Co$_{0.75}$Al$_{0.25}$-LDH thin-film electrode, which shows the best performance with a specific capacitance of 2500 F/cm^3 (833 F/g) [54].

Although great improvement has been achieved, the practical application of LDHs still suffers from the poor rate capability due to its semiconductor nature. The combinations of LDHs and highly conductive materials are expected to provide higher conductivity than pure LDHs and offer a synergistic effect in capacitive performance [57,58]. A novel graphene nanosheet/NiAl-LDH composite fabricated by Zhang *et al.* showed a remarkable capacitance of 1255.8 F/g and capacitance retention of 94% after 1500 cycles [58]. Wu *et al.* fabricated a hybrid film with ultrathin NiCo-LDH nanosheets grown on Ni foam. The as-obtained hybrid electrode displayed a significantly enhanced specific capacitance (2435 F/g at 6 A/g) and energy density compared to electrode material synthesized with other alkali sources and oxidants [59]. But, as observed from the charge/discharge profile of NiCo-LDH/Ni composite, the flat potential regions along with sloping pseudocapacitive regions indicate a battery-type process, which will undermine the power capability of ECs. Recently, Ma *et al.* proposed a true superlattice lamellar nanocomposite of CoAl/Co-Ni LDH and graphene by direct restacking of LDH nanosheets and single-layer graphene (oxide) nanosheets (Fig. 7a) [55]. The molecular-scale arrangement of LDH nanosheets directly neighboring to conductive graphene in the superlattice substantially improved the charge-transfer efficiency. The obtained rGO/LDH composite show high capacitance, excellent electrochemical reversibility and

ideal capacitive charge/discharge behavior up to ∼100 Hz, suggesting a surface-controlled electrochemical process and good pseudocapacitive behavior, as described in the previous section (Fig. 7b and c).

LDHs represent some of the most promising electrode materials due to their facile preparation/modification, good tunability and cost-effectiveness. However, it remains a challenge to precisely manipulate the LDHs into arbitrary nanoarchitectures, in order to achieve an accurate tailoring of the LDH electronic structure and architecture on multi-scale levels; and detailed insights into the electrochemical reaction processes are not well developed.

Conducting polymers

Conducting polymers are another kind of promising electrode material for PC due to their high conductivity (∼100−1000 S/m), fast doping/de-doping capability and excellent electrochemical reversibility. The application of conducting polymers as supercapacitor electrodes was first reported in 1963 by McNeill and co-workers [60]. The electron delocalization in $\pi-$orbital conjugation along the polymer backbone gives the compounds the ability to be oxidized or reduced at the surface [61]. Among various conducting polymers, polypyrrole (PPy), polyaniline (PANI), poly (styrene sulfonate), poly (3,4-ethylenedioxythiophene) (PEDOT), polythiophene and polymethyl methacrylate are most studied as electrodes for PCs. They exhibit large pseudocapacitances in the range typically between 500 to 3400 F/g, which is substantially larger than conventional carbon materials and comparable to metal oxides [61,62]. However, one drawback with these materials is the high ESR that resulted from the random deposition in the manufacturing process, which significantly slows down the ion diffusion within the entire electrode. To overcome this problem, conducting polymers are usually combined with other materials to construct composites with high conductivity and large SSA. Particular interest has been paid to CNTs and graphene due to their strong mechanical ability [63–65]. For example, Lu *et al.* prepared a film electrode of PPy/carbon nanotube (CNT)/graphene composite with PPy/CNT homogeneously distributed between graphene sheets (Fig. 7d) [56]. In such a layered structure, CNT and graphene not only provide high conductivity, but also construct a porous structure for ion diffusion. The study found that the PPy/CNT/graphene composite exhibited large capacitance as well as good rate capability (Fig. 7e). Lately, Hu *et al.* reported porous NiO/Ni(OH)$_2$/PEDOT nanocomposites (PNCs) on contra wires for fiber-shaped flexible solid-state ASC [66]. The ASC use a polymer gel as the electrode, the PNC/PEDOT as the cathode and the CMK-3 as the anode. The fiber-shaped ASC shows an operating voltage as high as 1.5 V. A high specific capacitance of 3.16 F/cm^3 and a high energy density of 1.1 m Wh/cm^3 are obtained.

The major obstacle inhibiting the real application of conducting polymers is their cycle instability due to the repeated swelling and shrinking due to the doping/de-doping of ions during charge/discharge [67,68]. A lot of methods have been reported to improve the cycling performance of polymer-based electrodes. Organic molecule doping, such as sulfanic acid azochromotrop and trion, were demonstrated to improve the capacitance retention of conducting polymers to more than 90% after 1000 cycles [69,70]. Also, coating conducting polymers with stable materials, such as titanium dioxide [67] or Nafion [68], was also effective in improving the cycling performance. However, these electro-inert materials in the composite will lower the conductivity and capacitance of the whole composite. Recently, Li *et al.* proposed coating the PANI and PPy nanowire with a thin carbonaceous shell. The structures of PANI and PPy were therefore maintained and large capacitance as well as high capacitance retention (95% and 85% after 10 000 cycles, respectively) were exhibited [71].

INTERCALATION PSEUDOCAPACITIVE ELECTRODE MATERIALS

In the past few years, research focus is directed toward the development of hybrid electrochemical capacitors (HECs), which asymmetrically and simultaneously store charges by surface ion adsorption/desorption on cathode and by lithium/sodium-de/intercalation in the anode. HECs, including lithium-ion capacitors (LICs) and sodium-ion capacitors (NICs), are expected to bridge the gap between high-energy LIBs/sodium-ion batteries (SIBs) and high-power ECs, becoming the ultimate power source for electric vehicles and uninterruptible power systems [72,73]. One of the major issues for HECs, however, is the imbalance in the charge/discharge rate between the two electrodes due to the intrinsic differences in the energy-storage mechanisms. Under the normal operating conditions of a HEC, this imbalance in the kinetics prevents full energy utilization of the intercalation electrode and imposes a high overpotential in the capacitive electrode, thus deteriorating the overall efficiency. Using high-rate-intercalation

pseudocapacitive materials as the anode is promising to balance the kinetics and power capability of both electrodes. The insertion-type materials are broadly classified into metal oxides, lithium/sodium metal oxide-based composites, transition metal carbides, transition metal dichalcogenides and so on. Particularly, some kinds of electrode material, such as lithium and sodium metal based materials and rutile TiO_2, cannot be defined as pseudocapacitive materials because of their voltage plateaus and phase changes during the de(intercalation) process. But their high rate capabilities ensure their applicability as high-rate electrodes in hybrid capacitors. Therefore, we discuss the preparation and application of these materials together in the following section.

Metal oxides

The different crystal structures of TiO_2 are formed by the stacking of TiO_6 octahedra in different ways [4], therefore leading to different electrochemical performance for electrochemical energy storage. Among TiO_2 of different phases, the anatase phase TiO_2 is most widely evaluated as an insertion-type anode for lithium-ion storage. Morphological optimization has been demonstrated to be an effective method to facilitate the ionic transport. For example, adoption of mesoporous TiO_2 microspheres as anode materials for LIC coupled with AC cathode led to an energy density as high as 79.3 Wh/kg and excellent cycling stability [72]. Fan *et al.* reported a LIC based on a TiO_2 anode and a graphene hydrogel cathode achieved maximum energy and power densities of 82 Wh/kg and 19 kW/kg, respectively [74]. It has also been demonstrated that the structure adjustment of nanocrystalline TiO_2 may change the charge-storage mechanism, leading to a faradic process occurring at the surface [75]. Dunn *et al.* used detailed CV technology to quantify the dependence of the faradic contribution on the size of nanocrystalline TiO_2. The results showed that the faradic contribution to charge storage increases tremendously for particle sizes under 10 nm, leading to higher levels of stored charge and much faster charge/discharge kinetics than lithium intercalation.

To address the problem of low conductivity, conductive additives were added to different polymorphs of TiO_2 [76,77]. Kang *et al.* constructed a HEC with anatase TiO_2-reduced graphene oxide (rGO) as the anode and AC cathode [78]. The LIC delivered high energy density ($\sim$42 Wh/kg), high power density ($\sim$8000 W/kg) and long-term life cycle (over 10 000 cycles). However, no optimization carried out in the materials will lead to less energy for the whole device, which is not a favorable op-

tion. Other methods, including introducing oxygen deficiency through hydrogenation and heteroatoms doping, may be optional strategies to achieve this aim.

Compared to anatase TiO_2, bronze phase (TiO_2-B) exhibits a lower Li-insertion potential ($\sim$1.55 V *vs.* Li), higher theoretical capacity of 335 mAh/g and less irreversible capacity loss in the first cycle [79,80]. In addition, TiO_2-B has an open tunnel framework and considerable interlayer space, which allows faster Li-ion diffusion in the bulk state. Therefore, TiO_2-B is regarded as a promising anode for HEC. The pseudocapacitive behavior of TiO_2-B bulk was first investigated by Kavan *et al.* [79]. They hold the view that lithium storage in TiO_2-B is controlled by pseudocapacitive behavior. Later, Che *et al.* prepared a porous TiO_2-B nanosheet with 5−10 nm thickness [80], which delivered a high capacity of 332 mAh/g at 0.1 C (1C = 335 mA/g) and 202 mAh/g at 10 C. This excellent rate capability can be attributed to its pseudocapacitive behavior for the fast deinsertion/insertion reaction of Li^+ and ultrathin nanosheets with porous structures which are able to enlarge the surface area. Despite these advantages, the sluggish ionic transport and poor electronic conductivity of TiO_2-B derived from its intrinsic property still need to be improved. Another kind of Ti-based oxide material, hydrogen titanates (such as $H_2Ti_3O_7$, $H_2Ti_6O_{13}$), have been demonstrated to be excellent anodes for HEC [81,82] (Fig. 8a). Investigations of the electrochemical behavior of hydrogen titanates using CV technology indicate that the charge storage is pseudocapacitive in nature [81] (Fig. 8b and c). A LIC was fabricated by using $H_2Ti_6O_{13}$ nanowires as anodes and ordered mesoporous carbon (CMK-3) as the cathode in an organic electrolyte with a voltage range of 1.0–3.5 V. The CMK-3//$H_2Ti_6O_{13}$ LIC exhibited maximum energy density and power density of 90 Wh/kg and 11 000 W/kg, respectively.

Recently, niobium pentoxide (Nb_2O_5), especially orthorhombic T-Nb_2O_5 (ortho-Nb_2O_5), has been considered as one of the most promising insertion-type anodes. According to the redox couple of Nb^{5+}/Nb^{4+}, charge storage occurs up to 2 Li^+/T-Nb_2O_5 for a maximum capacity of $\sim$200 mAh/g (720 C/g). T-Nb_2O_5 demonstrated high rate capability because the intercalation pseudocapacitive behavior of Li^+ (Na^+) occurs on the surface (even bulk) of the electrode without phase transition (Fig. 8d and e) [83]. Dunn *et al.* found that engineering at/beyond the nanoscale is the key to preserving the atomic-scale behavior for intercalation pseudocapacitance [4,83,85]. However, the poor electronic conductivity of T-Nb_2O_5 nanocrystals ($\sim$3.4 $\times$ 10^{-6} S/cm) may limit their
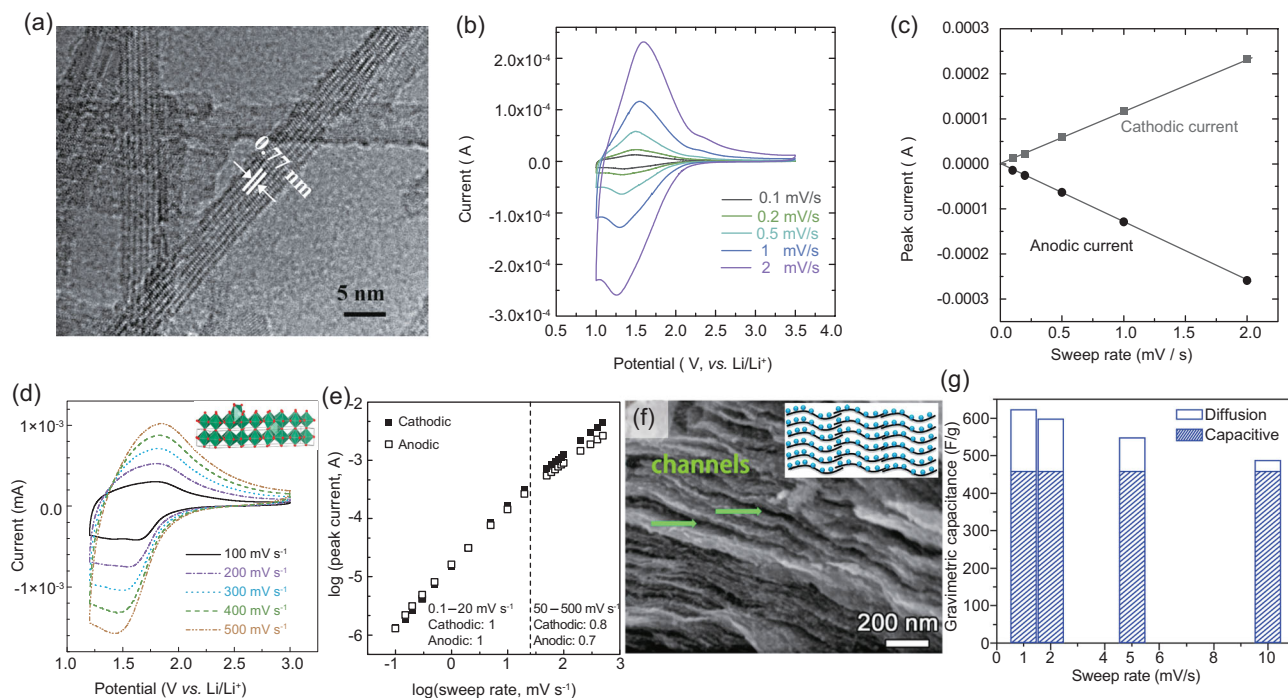
Figure 8. (a) High-resolution TEM (HRTEM) image of $H_2Ti_6O_{13}$-nanowires [81] (Copyright 2012, John Wiley & Sons, Inc.). (b) CV curves at various sweep rates and (c) the relationship between peak current and sweep rate of titanate nanowires. (d) CV curves of T-Nb_2O_5 from 100 to 500 mV/s [83] (Copyright 2013, Nature Publishing Group). (e) *b*-value determination of the peak anodic and cathodic currents. (f) Cross-sectional SEM images of T-Nb_2O_5/graphene composite papers (the inset schematically shows the nanostructure of T-Nb_2O_5/grapheme) [84] (Copyright 2015, American Chemical Society). (g) Capacitive contribution of T-Nb_2O_5/graphene composite paper.

real application, especially for thick electrodes with high mass loadings. In this regard, Long *et al.* presented a simple hydrothermal-heat-treatment process to decorate T-Nb_2O_5 nanocrystals onto the surface of rGO. The T-Nb_2O_5/rGO nanocomposite exhibited high specific capacitance (626 C/g), outstanding rate performance and cycling stability [86]. In addition, they constructed a LIC using T-Nb_2O_5/rGO nanocomposite and mesoporous carbon as the anode and cathode, respectively, which delivered a high energy density of 16 Wh/kg at an ultrahigh power density of 45 kW/kg. Later, Long and co-workers demonstrated a facile polyol-mediated solvothermal strategy to assemble free-standing T-Nb_2O_5 nanodots/rGO composite papers with uniform nanoporous structure, high conductivity (~2.5 S/cm), high loading mass (74.2%) and high bulk density (1.55 g/cm^3) [84] (Fig. 8f). When evaluated as a free-standing electrode, the composite papers delivered an unprecedented gravimetric/volumetric capacitance of 620.5 F/g and 961.8 F/cm^3 at a sweep rate of 1 mV/s. Moreover, LIC using T-Nb_2O_5/rGO papers as anode and AC as cathode delivered high energy density (47 Wh/g) with excellent power density (18 kW/kg) and cycling stability (~93% capacitive retention after 2000 cycles) (Fig. 8g). Recently,

the same group investigated the effect of Nb_2O_5 crystalline phases on Li^+ intercalation behavior including pseudo-hexagonal (*TT*-), orthorhombic (*T*-), tetragonal (*M*-) and monoclinic (*H*-) phases. Electrochemical results show that the Li^+ intercalation process in all crystal phases Nb_2O_5 is capacitive behavior, but the Li^+ intercalation behavior is highly dependent upon crystal structure. The *M*- and *H*- phases exhibited higher capacity and rate performance than the *T*- and *TT*- phases, which should be due to the more ordered crystal structure of *M*- and *H*- Nb_2O_5 with the face-sharing large 2D connected channels that allow faster ion diffusion [87]. In addition, they demonstrated for the first time that another N-O compound, NbO_2, exhibits much better Li^+ intercalation kinetics than Nb_2O_5 [88]. Lee *et al.* have demonstrated that ortho-Nb_2O_5 was also one of the promising anode materials with outstanding Na-ion energy storage as a result of de/intercalation reactions combined with a capacitive contribution after amorphization during the first discharge process [89]. Later, they reported a high-performance NIC based on Nb_2O_5@carbon core–shell nanoparticles and rGO nanocomposite anode and AC cathode [73]. The NIC delivered high energy and power density of 76 Wh/kg and 20 800 W/kg with a long-term stability in the voltage range of 1.0–4.3 V.

Vanadium pentoxide (V_2O_5) is very attractive for electrochemical energy storage due to the multiple oxidation states of V with high theoretical capacity of over 325 mAh/g ($>$2.2 mol of Li) and the ability to form layered compounds. Both amorphous and nanocrystalline forms of V_2O_5 can present pseudocapacitive behavior as evidenced by sloping charge–discharge curves during galvanostatic cycling and broad, featureless CVs. However, the pseudocapacitance of V_2O_5 is strongly dependent upon exposure of the active surface area to the electrolyte. This behavior is one property of extrinsic pseudocapacitive materials. Lu *et al.* fabricated a high-energy-density LIC containing thick-film electrode (over 100 μm) of V_2O_5 nanowires/CNT composite anode and commercial AC cathode in organic electrolyte [90]. The AC//V_2O_5/CNT showed a high energy density of 40 Wh/kg at a power density of 210 W/kg and a maximum power density of 20 kW/kg. They also demonstrated fast, reversible Na-ion energy storage in V_2O_5/CNT nanocomposite electrodes [91]. Various analytical technologies show that Na-ion storage in this material arises from a pseudocapacitive process. For example, the calculation based on Equation (5) indicated that, at a sweep rate of 10 mV/s, the capacitive contribution of the V_2O_5/CNT nanocomposite electrode is about 82%, which is dominant in the Na-ion storage process. Using a V_2O_5/CNT electrode as the anode and AC as the cathode, they fabricated NIC with 1 M $NaClO_4$ in propylene carbonate (PC) as the electrolyte. The NIC delivered maximum energy density of about 40 Wh/kg at an operated voltage of 2.8 V. The availability of capacitive storage based on Na-ion hybrid systems is an attractive, cost-effective alternative to Li-ion hybrid systems.

Lithium/sodium metal oxide-based electrode

The lithium titanate and sodium titanate, primarily $Li_4Ti_5O_{12}$ and $Na_2Ti_3O_7$, are considered as promising insertion-type anodes for HEC. As a 'zero-strain' insertion material, spinel $Li_4Ti_5O_{12}$ has received particular interest for electrochemical energy storage. The non-aqueous LIC was first presented by Amatucci *et al.* using nanostructured $Li_4Ti_5O_{12}$ as anode and AC as cathode in 2001 [92]. However, the low electronic conductivity ($\sim$$10^{-13}$ S/cm) remains a major obstacle for its practical application in LICs. The most commonly used strategies are engineering the nanostructure of electroactive particles, coating conductive layers on the surface and doping with appropriate ions/atoms. For example, Zhang *et al.* proposed a solid-state route to fabri-

cate Ti^{3+} self-doped $Li_4Ti_5O_{12}$ by using Ti_2O_3 as the precursor without any reducing agent [93]. A high-performance LIC was fabricated using Ti^{3+} self-doped $Li_4Ti_5O_{12}$ as the anode and AC derived from outer peanut shell as the cathode, which delivered high energy density (maximum, 67 Wh/kg) and high power density (maximum, 8000 W/kg). Additionally, the AC//LTO still retained about 79% of its original capacity, even after the 5000th cycle at 0.5 A/g.

As a promising anode for NICs, $Na_2Ti_3O_7$ exhibits a theoretical capacity of $\sim$200 mAh/g at an average insertion potential of 0.3 V (*vs.* Na/Na^+). Like other oxides, the low electronic conductivity limits the practical application of $Na_2Ti_3O_7$ in Na-ion energy storage. In order to enhance the kinetic response of $Na_2Ti_3O_7$, Zhang *et al.* used an applicable route to grow $Na_2Ti_3O_7$ *in situ* on CNTs (NTO@CNT) [94]. Kinetics analysis based on Equation (5) reveals an interesting pseudocapacitive behavior in the NTO@CNT electrode. For example, $\sim$52.7% of the total capacity comes from capacitive contribution at a scan rate of 0.6 mV/s, which is highly beneficial to fast Na^+ diffusion and long-term cyclability. Moreover, a high-performance NIC was also fabricated by using NTO@CNT as the anode and AC as the cathode, which delivered high energy density (58.5 W h/kg), high power density (3 kW/kg) and long-term cyclability ($\sim$75% of its original capacity at 0.4 A/g after 4000 cycles). Recently, a high-performance NIC with flexibility was constructed using 3D $Na_2Ti_3O_7$ nanosheet arrays/carbon textiles (NTO-NHAs/CT) as anodes and rGO films (GF) as cathodes (Fig. 9a) [95]. The flexible NIC delivered a high energy density of about 55 Wh/kg and high power density of 3000 W/kg with a voltage range of 1–3 V (Fig. 9b–d). Taking the fully packaged flexible NIC into consideration, the maximum volumetric energy density and power density reach up to 1.3 mWh/cm^3 and 70 mW/cm^3, respectively. Moreover, the flexible NIC demonstrated a stable electrochemical performance with almost 100% capacitance retention under harsh mechanical deformation.

Phosphate-based nanomaterials, such as $LiFePO_4$ [96] and $Na_3V_2(PO_4)_3$ [97], have been developed as important positive electrode materials for non-aqueous hybrid supercapacitors because of their high potential and high ionic diffusion coefficient. Lee *et al.* developed a sodium hybrid capacitor system based on carbon-coated $Na_3V_2(PO_4)_3$ (C-NVP) as the positive electrode and high-surface-area-activated carbons (CDCs) as the negative electrode [97]. Benefitting from the advantages of a high Na^+ diffusion coefficient, carbon-coated
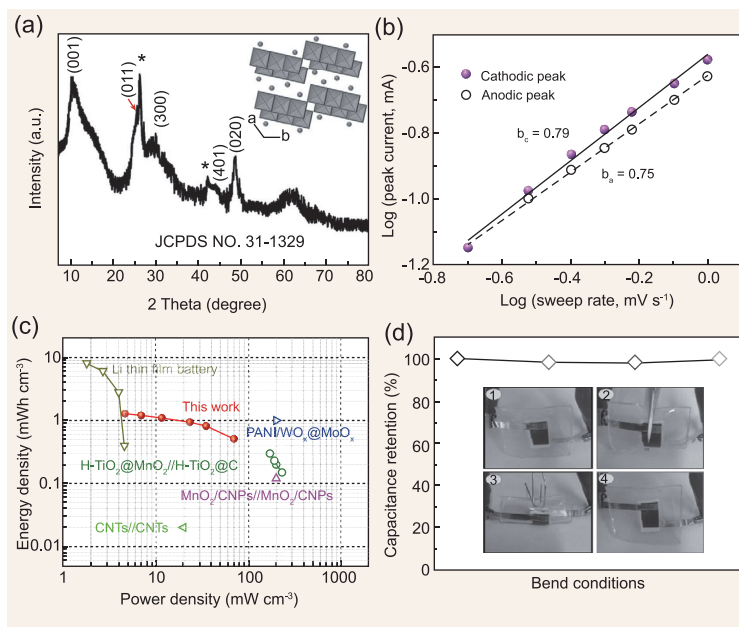
Figure 9. (a) XRD patterns of $Na_2Ti_3O_7$/carbon textiles. Inset: The crystallographic arrangements of $Na_2Ti_3O_7$. (b) Determination of *b*-value using the relationship between peak current of $Na_2Ti_3O_7$/carbon textiles electrode and sweep rates ranging from 0.2 to 1.0 mV/s. (c) Ragone plots based on the volume of flexible $Na_2Ti_3O_7$/carbon textiles//graphene NIC. The values reported for other flexible devices are added for comparison. (d) Capacitance retention of flexible NIC measured at 0.5 A/g under different bent conditions. Insets: Digital photographs of the flexible device in the respective bent conditions (Copyright 2016, John Wiley & Sons, Inc.).

nanostructure, porous properties and balanced electrode kinetics between positive and negative electrodes, the C-NVP/CDC hybrid supercapacitor exhibits a high energy density of 118 Wh/kg and power density of 850 W/kg and superior cyclic stability with 95% capacitance retention after 10 000 cycles. Besides, sodium metal phosphates, $NaMPO_4$ (M = Ni, Co, Mn) is another representative type of phosphate-based nanomaterials. Selvan *et al.* reported a solution combustion synthesis method to prepare the sodium metal phosphates [98]. They investigated the influence of electrolyte anions (Cl^-, SO_4^{2-}, OH^- and NO_3^-) and pH of the electrolyte solution on the performance of $NaMPO_4$ and found that the $NaMPO_4$ (M = Ni, Co, Mn) shows a highest specific capacitance when tested in 1 M NaOH electrolyte. Furthermore, $NaNiPO_4$ possesses higher capacitance compared to $NaCoPO_4$ and $NaMnPO_4$. An asymmetric supercapacitor ($AC//NaNiPO_4$) was further constructed and demonstrated a high specific capacitance of 56 F/g, leading to an energy density of 20 Wh/kg. Notably, the application of phosphate-based nanomaterials in non-aqueous hybrid supercapacitors seems to attract more attention.

Transition metal carbide

The volumetric performance of electrochemical energy-storage devices is attracting increasing attention due to the fast development of increasing demand for portable and wearable electronics [91]. Transition metal carbides (MXenes) is a novel family of electrode materials for supercapacitors, which are prepared by selective etching of the A element from the layered hexagonal MAX phases, where M represents a transition metal (e.g. Ti, V, Nb, etc.), A stands for an A-group element (e.g. Al, Si, In, Sn, etc.) and X is C and/or N (Fig. 10a) [99–101]. MXenes combine 2D conductive carbide layers with a hydrophilic, primarily hydroxyl-terminated surface. The rich chemistries and unique morphologies of MXenes, in addition to their good electronic conductivities, render them strong candidates for ECs.

Gogotsi *et al.* first demonstrated the spontaneous intercalation of cations from aqueous electrolyte between 2D Ti_3C_2 MXene layers [100]. A flexible, additive-free and conductive $Ti_3C_2T_x$ paper electrode could fabricate through easily filtering delaminated few-layer Ti_3C_2 (Fig. 10b). The $Ti_3C_2T_x$ paper electrode instead of multilayer exfoliated $Ti_3C_2T_x$ in the potassium hydroxide (KOH) electrolyte roughly doubled the gravimetric capacitance. Even more impressively, as shown in Fig. 10c, the volumetric capacitance values recorded for the paper were in the order of 340 F/cm^3, which are much higher than those for the porous carbon electrode. The *in situ* XRD studies revealed that electrochemical cycling leads to insignificant changes in the interlayer distance (*c*-value) of multilayer exfoliated $Ti_3C_2T_x$. When a $Ti_3C_2T_x$ electrode was cycled in a KOH-containing electrolyte, the *c*-values fluctuated within 0.33 Å as the potential was scanned from –1 to –0.2 V (Fig. 10d). MXenes can hold ions for much larger than Li^+, including Na^+, K^+, NH_4^+, Mg^{2+}, Ca^{2+} and Al^{3+}, which greatly expands the application range for an energy-storage device. As highlighted in this work, MXenes have demonstrated their potential as promising electrode materials for supercapacitors with volumetric capacitance exceeding all carbon materials.

Usually, fast ion adsorption response in supercapacitors enables fast energy storage and delivery, while ion intercalation in battery-like materials leads to larger amounts of energy stored, but at relatively lower rates due to ion diffusion limitation. The high capacity and good rate capability of MXenes seem to be a paradox. Levi and co-workers combined methodology of electrochemical quartz-crystal admittance (EQCA), *in situ* electronic conductance and electrochemical impedance spectrum to investigate the intercalation kinetics to
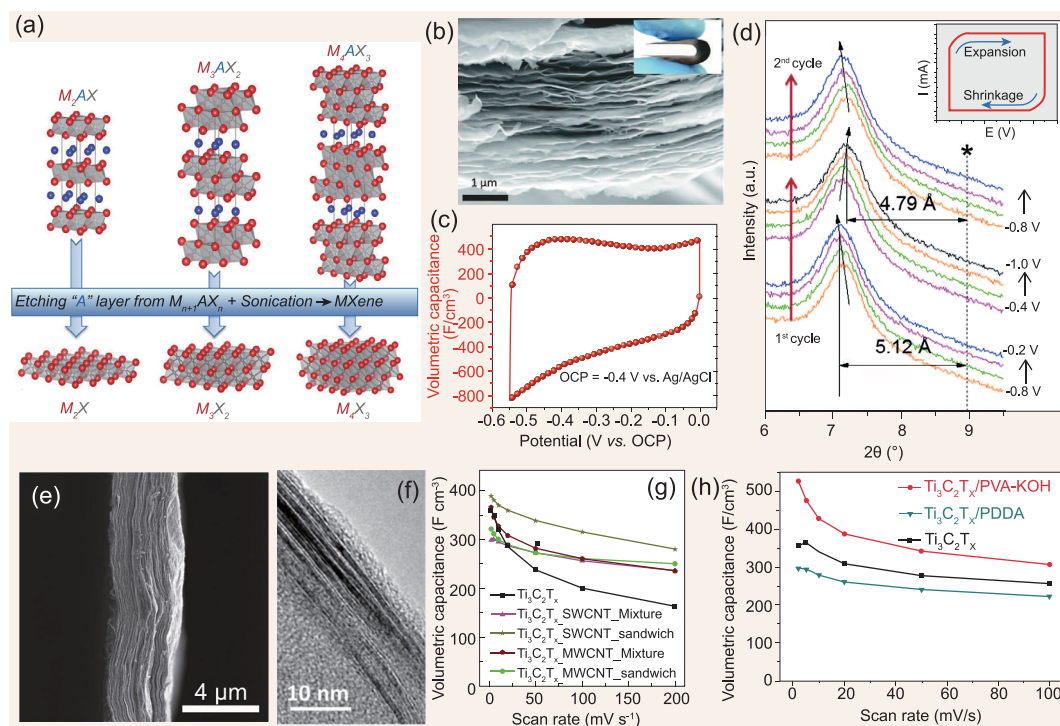
Figure 10. (a) Structure of MAX phases and the corresponding MXenes [99] (Copyright 2014, John Wiley & Sons, Inc.). (b) SEM image of $Ti_3C_2T_x$ paper electrode (inset is a photograph of the paper showing its flexibility) [100] (Copyright 2013, The American Association for the Advancement of Science). (c) Cycling performance of $Ti_3C_2T_x$ paper electrode (inset shows galvanostatic profiles at 1 A/g). (d) Electrochemical *in situ* XRD study of exfoliated $Ti_3C_2T_x$ in 1 M KOH electrolyte. (e) Cross-sectional SEM images of sandwich-like $Ti_3C_2T_x$/SWCNT [102] (Copyright 2015, John Wiley & Sons, Inc.). (f) HRTEM image showing the cross-section of a $Ti_3C_2T_x$/PVA-KOH film [103] (Copyright 2014, The National Academy of Sciences of the United States of America). (g) Volumetric capacitances of different $Ti_3C_2T_x$ electrodes. (h) Volumetric capacitances of different $Ti_3C_2T_x$ paper electrodes.

explain this phenomenon [104]. Mechanical deformations along with the insertion kinetics of $Ti_3C_2T_x$ electrode materials at various states of charge with a large variety of cations (Li^+, Na^+, K^+, Cs^+, Mg^{2+}, Ca^{2+}, Ba^{2+} and three tetra-alkylammonium cations) during cycling was carried out. A conjecture was proposed that the multilayer particles consist of shallow-adsorption sites near the edges and deep-adsorption sites with higher activation energies for ion adsorption in the interior of the particle. More work is ongoing to verify this constructure. To further improve the utilization of electroactive sites in MXenes, various strategies have been used to expand the interlayer distance between MXenes. One straightforward strategy that has been extensively investigated for improving the electrochemical performance of 2D nanomaterials is introducing interlayer spacers. For example, Gogotsi *et al.* showed that $Ti_3C_2T_x$ flakes mixed with carbon nanotubes or polymers could produce multifunctional paper electrodes with attractive mechanical and electrochemical properties (Fig. 10e and f). For example, sandwich-like MXene/CNT papers exhibited significantly higher gravimetric and

volumetric capacitances and excellent rate performances compared with pure MXene [103]. A high gravimetric capacitance of 150 F/g and volumetric capacitance of 390 F/cm^3 were measured for the sandwich-like MXene/SWCNT papers at a scan rate of 2 mV/s (Fig. 10g) [102]. Introducing KOH into the $Ti_3C_2T_x$/PVA film dramatically prevents the restacking of $Ti_3C_2T_x$ flakes and improves ionic transport and access to $Ti_3C_2T_x$, thus rendering volumetric specific capacitances of 528 F/cm^3 at 2 mV/s and 306 F/cm^3 at 100 mV/s (Fig. 10h). From a practical point of view, these values underscore the great potential for using MXenes in ECs with high gravimetric and volumetric performances. However, the chemical stability of MXenes in aqueous electrolyte still needs more investigation. As reported in recent work, few-layer $Ti_3C_2T_x$ nanosheets could be transformed into TiO_2 under atmospheric and hydrothermal conditions [105,106].

The unique properties of MXenes, including a 2D-layered structure and high electrical conductivity, also render them strong candidates for ECs with non-aqueous electrolyte, such as LICs and
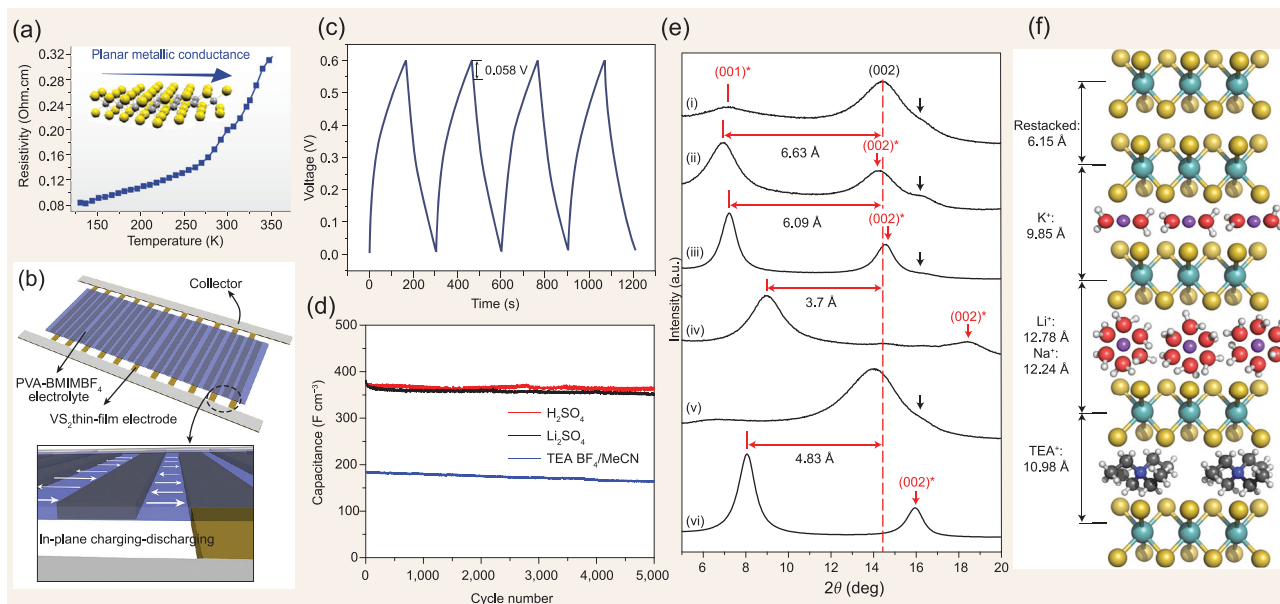
Figure 11. (a) Temperature dependence of planar resistivity of VS_2 thin film [108] (Copyright 2011, American Chemical Society). (b) Planar ion migration pathways for the in-plane supercapacitor and schematic illustration of the in-plane configuration of the as-fabricated supercapacitor. (c) Galvanostatic cycling behavior and IR drop illustration of VS_2 thin-film-based supercapacitor. (d) Capacitance retention of 1T phase MoS_2 nanosheet paper after 5000 cycles in 0.5 M Li_2SO_4, H_2SO_4 and 1 M $TEABF_4$ in acetonitrile [109] (Copyright 2015, Nature Publishing Group). (e) XRD spectra from as-exfoliated 1T phase MoS_2 nanosheets (i) and cycled MoS_2 film in different sulfate-based electrolytes: Li_2SO_4 (ii), Na_2SO_4 (iii), K_2SO_4 (iv), H_2SO_4 (v) and in $TEABF_4$/MeCN organic electrolyte (vi). (f) Schematics of restacked non-intercalated and intercalated 1T MoS_2 nanosheets. Different spacings were measured by XRD depending on the hydrated intercalated ion.

sodium-ion capacitors. Ti_2C was adopted as an anode to assemble a non-aqueous asymmetric cell with AC as the counter electrode. The material exhibited a capacity of 65 mAh/g at 10°C and no diffusion limitation was shown at rates below 5 mV/s. The asymmetric cell exhibited a maximum energy density of 30 Wh/kg at 930 W/kg for 1000 cycles. These studies indicated that Li^+ ions are easily accessed to the electroactive sites in MXenes. Recently, Yamada and Wang *et al.* demonstrated that Ti_2C nanosheets achieved a reversible capacity of 175 mAh/g at an average operating potential of 1.3 V (*vs.* Na/Na^+) and good cycle stability (19% losses of second capacity after 100 cycles) [107]. Moreover, a high-power sodium-ion hybrid capacitor was fabricated by using MXene Ti_2C as an anode and alluaudite $Na_2Fe_2(SO_4)_3$ as a cathode. The $Na_2Fe_2(SO_4)_3$//Ti_2C prototype capacitor operates at a relatively high voltage of 2.4 V and delivers an outstanding energy density of 260 Wh/kg at an ultrahigh power density of 14 000 W/kg (based on the weight of the Ti_2C anode), which overcomes the trade-off limit between high energy and high power. The prominent electrochemical performance of MXenes renders them as a promising candidate for use in asymmetric various hybrid energy-storage devices.

Transition metal sulfide

Transition metal dichalcogenides (TMDs) can be generally described using a formula of MX_2, where M is a transition metal (typically from groups IV–VII) and X is a chalcogen such as S, Se or Te [108,110–113]. TMDs usually exist in a graphite-like layered structure which consists of a hexagonally packed layer of metal atoms sandwiched between two layers of chalcogen atoms. Typically, each layer has a thickness of 0.6−0.7 nm, exhibiting high conductivity that is similar to that of graphene [112]. Some of the layered TMDs, such as MoS_2, VS_2 and WS_2, have played an increasingly crucial role in materials science and engineering for applications in ECs [108,109,114,115]. For example, Wu *et al.* prepared a single trilayer of VS_2 through exfoliation by NH_3 intercalation and applied them to build flexible all-solid micro-supercapacitors (Fig. 11a and b) [108]. The obtained device obtained a planar capacitance of 4760 $\mu F/cm^2$ using the ionic liquid $BMIMBF_4$ as electrolyte (Fig. 11c). The supercapacitor also demonstrated excellent cycling stability with negligible loss of capacitance after 1000 charge/discharge cycles. Another brilliant example of using the TMDs in the application of EC was demonstrated by the chemical exfoliated 1T phase

MoS$_2$ which shows much enhanced capacitive properties. In this work, the 1T-MoS$_2$ showed excellent abilities to intercalate cations, such as H$^+$, Na$^+$, K$^+$ and Li$^+$, achieving volumetric capacitance values of between 400 and 700 F/cm^3 in both aqueous and organic electrolytes (Fig. 11d–f) [109]. Layered TMDs will show different electrochemical properties which depend on their elemental composition, crystal structure, size and defects. Therefore, we can envision that doping and chemical modifications of the surface/edges of TMDs will lead to enhanced electrochemical properties.

SUMMARY AND OUTLOOK

Pseudocapacitive electrodes are promising to dramatically promote the capacitance of ECs for their faradic charge-storage process. HECs with pseudocapacitive electrodes as anodes can achieve high energy density that is comparable to that of batteries. But the problem for this kind of materials is the relatively low conductivity and slow ion transfer, which may cause deterioration in the rate capability and cycle stability. Until now, nanostructuration, combined with highly conductive materials and surface doping, is the most widely used strategy to improve the conductivity and facilitate ion transfer in pseudocapacitive electrodes. However, some charge-storage mechanisms are still unclear and worthy of deep investigation. Studies combining electrochemical techniques and various spectrometric methods may be needed. To advance the performance of the full device, in addition to the electrode materials, the electrolyte and separator used in hybrid supercapacitors need to be taken into consideration. Furthermore, observing the self-discharge and leakage current is needed, which are also important criteria for energy-storage devices. Additionally, when the pseudocapacitive materials are applied in device application, the fabrication techniques of electrodes, including the weight loading and the thickness of the electrode, should be addressed. It may be misleading to regard a material as a high-energy-density pseudocapacitor when low mass loadings or thin films are used and charge/discharge experiments are conducted over tens of minutes.

FUNDING

REFERENCES

1. Conway BE. *Electrochemical Supercapacitors: Scientific Fundamentals and Technological Applications.* New York: Kluwer-Academic, 1999.
2. Burke A. Ultracapacitors: why, how, and where is the technology. *J Power Sources* 2000; **91**: 37–50.
3. Miller JR and Simon P. Electrochemical capacitors for energy management. *Science* 2008; **321**: 651–2.
4. Augustyn V, Simon P and Dunn B. Pseudocapacitive oxide materials for high-rate electrochemical energy storage. *Energy Environ Sci* 2014; **7**: 1597–614.
5. Dubal D, Ayyad O and Ruiz V *et al.* Hybrid energy storage: the merging of battery and supercapacitor chemistries. *Chem Soc Rev* 2015; **44**: 1777–90.
6. Conway BE. Transition from 'supercapacitor' to 'battery' behavior in electrochemical energy storage. *J Electrochem Soc* 1991; **138**: 1539–48.
7. Conway B, Birss V and Wojtowicz J. The role and utilization of pseudocapacitance for energy storage by supercapacitors. *J Power Sources* 1997; **66**: 1–14.
8. Liu TC, Pell W and Conway B *et al.* Behavior of molybdenum nitrides as materials for electrochemical capacitors comparison with ruthenium oxide. *J Electrochem Soc* 1998; **145**: 1882–8.
9. Ardizzone S, Fregonara G and Trasatti S. 'Inner' and 'outer' active surface of RuO$_2$ electrodes. *Electrochim Acta* 1990; **35**: 263–7.
10. Lin T, Chen I-W and Liu F *et al.* Nitrogen-doped mesoporous carbon of extraordinary capacitance for electrochemical energy storage. *Science* 2015; **350**: 1508–13.
11. Long JW, Swider KE and Merzbacher CI *et al.* Voltammetric characterization of ruthenium oxide-based aerogels and other RuO$_2$ solids: the nature of capacitance in nanostructured materials. *Langmuir* 1999; **15**: 780–5.
12. Makino S, Ban T and Sugimoto W. Electrochemical capacitor behavior of RuO$_2$ nanosheets in buffered solution and its application to hybrid capacitor. *Electrochemistry* 2013; **81**: 795–7.
13. Hu C-C, Chen W-C and Chang K-H. How to achieve maximum utilization of hydrous ruthenium oxide for supercapacitors. *J Electrochem Soc* 2004; **151**: A281–90.
14. Sugimoto W, Iwata H and Yokoshima *et al.* Proton and electron conductivity in hydrous ruthenium oxides evaluated by electrochemical impedance spectroscopy: the origin of large capacitance. *J Phys Chem B* 2005; **109**: 7330–8.
15. Xu H, Hu X and Sun Y *et al.* Flexible fiber-shaped supercapacitors based on hierarchically nanostructured composite electrodes. *Nano Res* 2015; **8**: 1148–58.
16. Wang X, Wang X and Huang W *et al.* Sol–gel template synthesis of highly ordered MnO$_2$ nanowire arrays. *J Power Sources* 2005; **140**: 211–5.

17. Toupin M, Brousse T and Bélanger D. Charge storage mechanism of MnO_2 electrode used in aqueous electrochemical capacitor. *Chem Mater* 2004; **16**: 3184–90.

18. Lang X, Hirata A and Fujita T *et al.* Nanoporous metal/oxide hybrid electrodes for electrochemical supercapacitors. *Nat Nanotech* 2011; **6**: 232–6.

19. Zhang F, Yuan C and Lu X *et al.* Facile growth of mesoporous Co_3O_4 nanowire arrays on Ni foam for high performance electrochemical capacitors. *J Power Sources* 2012; **203**: 250–6.

20. Liu J, Jiang J and Cheng C *et al.* Co_3O_4 Nanowire@MnO_2 ultrathin nanosheet core/shell arrays: a new class of high-performance pseudocapacitive materials. *Adv Mater* 2011; **23**: 2076–81.

21. Huang L, Chen D and Ding Y *et al.* Nickel–cobalt hydroxide nanosheets coated on $NiCo_2O_4$ nanowires grown on carbon fiber paper for high-performance pseudocapacitors. *Nano Lett* 2013; **13**: 3135–9.

22. Meher SK and Rao GR. Effect of microwave on the nanowire morphology, optical, magnetic, and pseudocapacitance behavior of Co_3O_4. *J Phys Chem C* 2011; **115**: 25543–56.

23. Yuan C, Zhang X and Su L *et al.* Facile synthesis and self-assembly of hierarchical porous NiO nano/micro spherical superstructures for high performance supercapacitors. *J Mater Chem* 2009; **19**: 5772–7.

24. Zhang F, Yuan C and Zhu J *et al.* Flexible films derived from electrospun carbon nanofibers incorporated with Co_3O_4 hollow nanoparticles as self-supported electrodes for electrochemical capacitors. *Adv Funct Mater* 2013; **23**: 3909–15.

25. Zhu YG, Wang Y and Shi Y *et al.* Phase transformation induced capacitance activation for 3D graphene-CoO nanorod pseudocapacitor. *Adv Energy Mater* 2014; **4**: 1301788.

26. Shen L, Che Q and Li H *et al.* Mesoporous $NiCo_2O_4$ nanowire arrays grown on carbon textiles as binder-free flexible electrodes for energy storage. *Adv Funct Mater* 2014; **24**: 2630–7.

27. Wei W, Cui X and Chen W *et al.* Manganese oxide-based materials as electrochemical supercapacitor electrodes. *Chem Soc Rev* 2011; **40**: 1697–721.

28. Kuo S-L and Wu N-L. Electrochemical characterization on $MnFe_2O_4$/carbon black composite aqueous supercapacitors. *J Power Sources* 2006; **162**: 1437–43.

29. Xu H, Hu X and Yang H *et al.* Flexible asymmetric micro-supercapacitors based on Bi_2O_3 and MnO_2 nanoflowers: larger areal mass promises higher energy density. *Adv Energy Mater* 2015; **5**: 1401882.

30. Hou L, Yuan C and Yang L *et al.* Urchin-like Co_3O_4 microspherical hierarchical superstructures constructed by one-dimension nanowires toward electrochemical capacitors. *RSC Adv* 2011; **1**: 1521–6.

31. Bao L, Zang J and Li X. Flexible Zn_2SnO_4/MnO_2 core/shell nanocable-carbon microfiber hybrid composites for high-performance supercapacitor electrodes. *Nano Lett* 2011; **11**: 1215–20.

32. Tao F, Zhao Y-Q and Zhang G-Q *et al.* Electrochemical characterization on cobalt sulfide for electrochemical supercapacitors. *Electrochem Commun* 2007; **9**: 1282–7.

33. Zhu T, Wang Z and Ding S *et al.* Hierarchical nickel sulfide hollow spheres for high performance supercapacitors. *RSC Adv* 2011; **1**: 397–400.

34. Zhang H, Yu X and Guo D *et al.* Synthesis of bacteria promoted reduced graphene oxide-nickel sulfide networks for advanced supercapacitors. *ACS Appl Mater Interfaces* 2013; **5**: 7335–40.

35. Shen L, Yu L and Wu HB *et al.* Formation of nickel cobalt sulfide ball-in-ball hollow spheres with enhanced electrochemical pseudocapacitive properties. *Nat Commun* 2015; **6**: 6694.

36. Chen W, Xia C and Alshareef HN. One-step electrodeposited nickel cobalt sulfide nanosheet arrays for high-performance asymmetric supercapacitors. *ACS Nano* 2014; **8**: 9531–41.

37. Shen L, Wang J and Xu G *et al.* $NiCo_2S_4$ nanosheets grown on nitrogen-doped carbon foams as an advanced electrode for supercapacitors. *Adv Energy Mater* 2015; **5**: 1400977.

38. Choi D, Blomgren GE and Kumta PN. Fast and reversible surface redox reaction in nanocrystalline vanadium nitride supercapacitors. *Adv Mater* 2006; **18**: 1178–82.

39. Porto RL, Frappier R and Ducros J *et al.* Titanium and vanadium oxynitride powders as pseudo-capacitive materials for electrochemical capacitors. *Electrochim Acta* 2012; **82**: 257–62.

40. Xiao X, Peng X and Jin H *et al.* Freestanding mesoporous VN/CNT hybrid electrodes for flexible all-solid-state supercapacitors. *Adv Mater* 2013; **25**: 5091–7.

41. Ghimbeu CM, Raymundo-Piñero E and Fioux P *et al.* Vanadium nitride/carbon nanotube nanocomposites as electrodes for supercapacitors. *J Mater Chem* 2011; **21**: 13268–75.

42. Hanumantha PJ, Datta MK and Kadakia KS *et al.* A simple low temperature synthesis of nanostructured vanadium nitride for supercapacitor applications. *J Electrochem Soc* 2013; **160**: A2195–206.

43. Pang H, Ee SJ and Dong Y *et al.* TiN@VN nanowire arrays on 3D carbon for High-performance supercapacitors. *ChemElectroChem* 2014; **1**: 1027–30.

44. Xu Y, Wang J and Ding B *et al.* General strategy to fabricate ternary metal nitride/carbon nanofibers for supercapacitors. *ChemElectroChem* 2015; **2**: 2020–6.

45. Lu X, Yu M and Zhai T *et al.* High energy density asymmetric quasi-solid-state supercapacitor based on porous vanadium nitride nanowire anode. *Nano Lett* 2013; **13**: 2628–33.

46. Saha S, Jana M and Khanra P *et al.* Band gap engineering of boron nitride by graphene and its application as positive electrode material in asymmetric supercapacitor device. *ACS Appl Mater Interfaces* 2015; **7**: 14211–22.

47. Wang Y, Yang W and Yang J. A Co–Al layered double hydroxides nanosheets thin-film electrode fabrication and electrochemical study. *Electrochem Solid-State Lett* 2007; **10**: A233–6.

48. Faour A, Mousty C and Prevot V *et al.* Correlation among structure, microstructure, and electrochemical properties of NiAl–CO_3 layered double hydroxide thin films. *J Phys Chem C* 2012; **116**: 15646–59.

49. Prevot V, Forano C and Khenifi A *et al.* A templated electrosynthesis of macroporous NiAl layered double hydroxides thin films. *Chem Commun* 2011; **47**: 1761–3.

50. Shao M, Zhang R and Li Z *et al.* Layered double hydroxides toward electrochemical energy storage and conversion: design, synthesis and applications. *Chem Commun* 2015; **51**: 15880–93.

51. Rozov K, Berner U and Taviot-Gueho C *et al.* Synthesis and characterization of the LDH hydrotalcite–pyroaurite solid-solution series. *Cement Concrete Res* 2010; **40**: 1248–54.

52. Whilton NT, Vickers PJ and Mann S. Bioinorganic clays: synthesis and characterization of amino-andpolyamino acid intercalated layered double hydroxides. *J Mater Chem* 1997; **7**: 1623–9.

53. Shao M, Ning F and Zhao Y *et al.* Core–shell layered double hydroxide microspheres with tunable interior architecture for supercapacitors. *Chem Mater* 2012; **24**: 1192–7.

54. Wang Y, Yang W and Chen C *et al.* Fabrication and electrochemical characterization of cobalt-based layered double hydroxide nanosheet thin-film electrodes. *J Power Sources* 2008; **184**: 682–90.

55. Ma R, Liu X and Liang J *et al.* Molecular-scale heteroassembly of redoxable hydroxide nanosheets and conductive graphene into superlattice composites for high-performance supercapacitors. *Adv Mater* 2014; **26**: 4173–8.

56. Lu X, Dou H and Yang S *et al.* Fabrication and electrochemical capacitance of hierarchical graphene/polyaniline/carbon nanotube ternary composite film. *Electrochim Acta* 2011; **56**: 9224–32.

57. Gao Z, Wang J and Li Z *et al.* Graphene nanosheet/Ni^{2+}/Al^{3+} layered double-hydroxide composite as a novel electrode for a supercapacitor. *Chem Mater* 2011; **23**: 3509–16.

58. Zhang L, Wang J and Zhu J *et al.* 3D porous layered double hydroxides grown on graphene as advanced electrochemical pseudocapacitor materials. *J Mater Chem A* 2013; **1**: 9046–53.

59. Chen H, Hu L and Chen M *et al.* Nickel-cobalt layered double hydroxide nanosheets for high-performance supercapacitor electrode materials. *Adv Funct Mater* 2014; **24**: 934–42.

60. McNeill R, Siudak R and Wardlaw J *et al.* Electronic conduction in polymers. I. The chemical structure of polypyrrole. *Aust J Chem* 1963; **16**: 1056–75.

61. Hall PJ, Mirzaeian M and Fletcher SI *et al.* Energy storage in electrochemical capacitors: designing functional materials to improve performance. *Energy Environ Sci* 2010; **3**: 1238–51.

62. Wang G, Zhang L and Zhang J. A review of electrode materials for electrochemical supercapacitors. *Chem Soc Rev* 2012; **41**: 797–828.

63. Wu Q, Xu Y and Yao Z *et al.* Supercapacitors based on flexible graphene/polyaniline nanofiber composite films. *ACS Nano* 2010; **4**: 1963–70.

64. Snook GA, Kao P and Best AS. Conducting-polymer-based supercapacitor devices and electrodes. *J Power Sources* 2011; **196**: 1–12.

65. Lu X, Dou H and Yang S *et al.* Fabrication and electrochemical capacitance of hierarchical graphene/polyaniline/carbon nanotube ternary composite film. *Electrochim Acta* 2011; **56**: 9224–32.

66. Yang H, Xu H and Li M *et al.* Assembly of NiO/Ni(OH)$_2$/PEDOT nanocomposites on contra wires for fiber-shaped flexible asymmetric supercapacitors. *ACS Appl Mater Interfaces* 2016; **8**: 1774–9.

67. Xie K, Li J and Lai Y *et al.* Polyaniline nanowire array encapsulated in titania nanotubes as a superior electrode for supercapacitors. *Nanoscale* 2011; **3**: 2202–7.

68. Kim B, Kwon J and Ko J *et al.* Preparation and enhanced stability of flexible supercapacitor prepared from Nafion/polyaniline nanofiber. *Synthetic Met* 2010; **160**: 94–8.

69. Chen S and Zhitomirsky I. Polypyrrole electrodes doped with sulfanilic acid azochromotrop for electrochemical supercapacitors. *J Power Sources* 2013; **243**: 865–71.

70. Shi K and Zhitomirsky I. Influence of current collector on capacitive behavior and cycling stability of Tiron doped polypyrrole electrodes. *J Power Sources* 2013; **240**: 42–9.

71. Liu T, Finn L and Yu M *et al.* Polyaniline and polypyrrole pseudocapacitor electrodes with excellent cycling stability. *Nano lett* 2014; **14**: 2522–7.

72. Cai Y, Zhao B and Wang J *et al.* Non-aqueous hybrid supercapacitors fabricated with mesoporous TiO$_2$ microspheres and activated carbon electrodes with superior performance. *J Power Sources* 2014; **253**: 80–9.

73. Lim E, Jo C and Kim MS *et al.* High-performance sodium-ion hybrid supercapacitor based on Nb$_2$O$_5$@carbon core–shell nanoparticles and reduced graphene oxide nanocomposites. *Adv Funct Mater* 2016; **26**: 3711–9.

74. Wang H, Guan C and Wang X *et al.* A high energy and oower Li-ion capacitor based on a TiO$_2$ nanobelt array anode and a graphene hydrogel gathode. *Small* 2015; **11**: 1470–7.

75. Wang J, Polleux J and Lim J *et al.* Pseudocapacitive contributions to electrochemical energy storage in TiO$_2$ (anatase) nanoparticles. *J Phys Chem C* 2007; **111**: 14925–31.

76. Chen Z, Yuan Y and Zhou H *et al.* 3D nanocomposite architectures from carbon-nanotube-threaded nanocrystals for high-performance electrochemical energy storage. *Adv Mater* 2014; **26**: 339–45.

77. Dziewoński PM and Grzeszczuk M. Towards TiO$_2$-conducting polymer hybrid materials for lithium ion batteries. *Electrochim Acta* 2010; **55**: 3336–47.

78. Kim H, Cho MY and Kim MH *et al.* A novel high-energy hybrid supercapacitor with an anatase TiO$_2$-reduced graphene oxide anode and an activated carbon cathode. *Adv Energy Mater* 2013; **3**: 1500–6.

79. Zukalova M, Kalbac M and Kavan L *et al.* Pseudocapacitive lithium storage in TiO$_2$ (B). *Chem Mater* 2005; **17**: 1248–55.

80. Liu S, Jia H and Han L *et al.* Nanosheet-constructed porous TiO$_2$-B for advanced lithium ion batteries. *Adv Mater* 2012; **24**: 3201–4.

81. Wang Y, Hong Z and Wei M *et al.* Layered H$_2$Ti$_6$O$_{13}$-Nanowires: a new promising pseudocapacitive material in non-aqueous electrolyte. *Adv Funct Mater* 2012; **22**: 5185–93.

82. Li J, Tang Z and Zhang Z. Layered hydrogen titanate nanowires with novel lithium intercalation properties. *Chem Mater* 2005; **17**: 5848–55.

83. Augustyn V, Come J and Lowe MA *et al.* High-rate electrochemical energy storage through Li$^+$ intercalation pseudocapacitance. *Nat Mater* 2013; **12**: 518–22.

84. Kong L, Zhang C and Wang J *et al.* Free-standing T-Nb$_2$O$_5$/graphene composite papers with ultrahigh gravimetric/volumetric capacitance for li-ion intercalation pseudocapacitor. *ACS Nano* 2015; **9**: 11200–8.

85. Brezesinski K, Wang J and Haetge J *et al.* Pseudocapacitive contributions to charge storage in highly ordered mesoporous group V transition metal oxides with iso-oriented layered nanocrystalline domains. *J Am Chem Soc.* 2010; **132**: 6982–90.

86. Kong L, Zhang C and Zhang S *et al.* High-power and high-energy asymmetric supercapacitors based on Li+-intercalation into a T-Nb$_2$O$_5$/graphene pseudocapacitive electrode. *J Mater Chem A.* 2014; **2**: 17962–70.

87. Kong L, Cao X and Wang J *et al.* Revisiting Li$^+$ intercalation into various crystalline phases of Nb$_2$O$_5$ anchored on graphene sheets as pseudocapacitive electrodes. *J Power Sources* 2016; **309**: 42–9.

88. Kong L, Zhang C and Wang J *et al.* Nanoarchitectured Nb$_2$O$_5$ hollow, Nb$_2$O$_5$@carbon and NbO$_2$@carbon core-shell microspheres for ultrahigh-rate intercalation pseudocapacitors. *Sci Rep* 2016; **6**: 21177.

89. Kim H, Lim E and Jo C *et al.* Ordered-mesoporous Nb$_2$O$_5$/carbon composite as a sodium insertion material. *Nano Energy* 2015; **16**: 62–70.

90. Chen Z, Augustyn V and Wen J *et al.* High-performance supercapacitors based on intertwined CNT/V$_2$O$_5$ nanowire nanocomposites. *Adv Mater* 2011; **23**: 791–5.

91. Chen Z, Augustyn V and Jia X *et al.* High-performance sodium-ion pseudocapacitors based on hierarchically porous nanowire composites. *ACS Nano* 2012; **6**: 4319–27.

92. Amatucci GG, Badway F and Du Pasquier A *et al.* An asymmetric hybrid non-aqueous energy storage cell. *J Electrochem Soc* 2001; **148**: A930–9.

93. Dong S, Wang X and Shen L *et al.* Trivalent Ti self-doped Li$_4$Ti$_5$O$_{12}$: a high performance anode material for lithium-ion capacitors. *J Electrochem Soc* 2015; **757**: 1–7.

94. Dong S, Shen L and Li H *et al.* Pseudocapacitive behaviours of $Na_2Ti_3O_7$@ CNT coaxial nanocables for high-performance sodium-ion capacitors. *J Mater Chem A* 2015; **3**: 21277–83.

95. Dong S, Shen L and Li H *et al.* Flexible sodium-ion pseudocapacitors based on 3D $Na_2Ti_3O_7$ nanosheet arrays/carbon textiles anodes. *Adv Funct Mater* 2016; **26**: 3703–10.

96. Naoi K, Kisu K and Iwama E *et al.* Ultrafast charge–discharge characteristics of a nanosized core–shell structured $LiFePO_4$ material for hybrid supercapacitor applications. *Energy Environ Sci* 2016; **9**: 2143–51.

97. Thangavel R, Kaliyappan K and Kang K *et al.* Going beyond lithium hybrid capacitors: proposing a new high-performing sodium hybrid capacitor system for next-generation hybrid vehicles made with bio-inspired activated carbon. *Adv Energy Mater* 2016; **6**: 1502199.

98. Senthilkumar B, Sankar KV and Vasylechko L *et al.* Synthesis and electrochemical performances of maricite-$NaMPO_4$ (M= Ni, Co, Mn) electrodes for hybrid supercapacitors. *RSC Adv* 2014; **4**: 53192–200.

99. Naguib M, Mochalin VN and Barsoum MW *et al.* MXenes: a new family of two-dimensional materials. *Adv Mater* 2014; **26**: 992–1005.

100. Lukatskaya MR, Mashtalir O and Ren CE *et al.* Cation intercalation and high volumetric capacitance of two-dimensional titanium carbide. *Science* 2013; **341**: 1502–5.

101. Naguib M, Kurtoglu M and Presser V *et al.* Two-dimensional nanocrystals produced by exfoliation of Ti_3AlC_2. *Adv Mater* 2011; **23**: 4248–53.

102. Zhao MQ, Ren CE and Ling Z *et al.* Flexible MXene/carbon nanotube composite paper with high volumetric capacitance. *Adv Mater* 2015; **27**: 339–45.

103. Ling Z, Ren CE and Zhao M-Q *et al.* Flexible and conductive MXene films and nanocomposites with high capacitance. *Proc Natl Acad Sci USA* 2014; **111**: 16676–81.

104. Levi MD, Lukatskaya MR and Sigalov S *et al.* Solving the capacitive paradox of 2D MXene using electrochemical quartz-crystal admittance and in situ electronic conductance measurements. *Adv Energy Mater* 2015; **5**: 1400815.

105. Naguib M, Mashtalir O and Lukatskaya MR *et al.* One-step synthesis of nanocrystalline transition metal oxides on thin sheets of disordered graphitic carbon by oxidation of MXenes. *Chem Commun* 2014; **50**: 7420–3.

106. Ying Y, Liu Y and Wang X *et al.* Two-dimensional titanium carbide for efficiently reductive removal of highly toxic chromium (VI) from water. *ACS Appl Mater Interfaces* 2015; **7**: 1795–803.

107. Wang X, Kajiyama S and Iinuma H *et al.* Pseudocapacitance of MXene nanosheets for high-power sodium-ion hybrid capacitors. *Nat Commun* 2015; **6**: 6544.

108. Feng J, Sun X and Wu C *et al.* Metallic few-layered VS_2 ultrathin nanosheets: high two-dimensional conductivity for in-plane supercapacitors. *J Am Chem Soc* 2011; **133**: 17832–8.

109. Acerce M, Voiry D and Chhowalla M. Metallic 1T phase MoS_2 nanosheets as supercapacitor electrode materials. *Nat Nanotech* 2015; **10**: 313–8.

110. Chhowalla M, Shin HS and Eda G *et al.* The chemistry of two-dimensional layered transition metal dichalcogenide nanosheets. *Nat Chem* 2013; **5**: 263–75.

111. Ma G, Peng H and Mu J *et al.* In situ intercalative polymerization of pyrrole in graphene analogue of MoS_2 as advanced electrode material in supercapacitor. *J Power Sources* 2013; **229**: 72–8.

112. Soon JM and Loh KP. Electrochemical double-layer capacitance of MoS_2 nanowall films. *Electrochem Solid-State Lett* 2007; **10**: A250–4.

113. Cao L, Yang S and Gao W *et al.* Direct laser-patterned micro-supercapacitors from paintable MoS_2 films. *Small* 2013; **9**: 2905–10.

114. Winchester A, Ghosh S and Feng S *et al.* Electrochemical characterization of liquid phase exfoliated two-dimensional layers of molybdenum disulfide. *ACS Appl Mater Interfaces* 2014; **6**: 2125–30.

115. Ratha S and Rout CS. Supercapacitor electrodes based on layered tungsten disulfide-reduced graphene oxide hybrids synthesized by a facile hydrothermal method. *ACS Appl Mater Interfaces* 2013; **5**: 11427–33.